





NOTICES

When Government drawings, specifications, or other data are used for any purpose other than in connection with a definitely related Government procurement operation, the United States Government thereby incurs no responsibility nor any obligation whatsoever, and the fact that the Government may have formulated, furnished, or in any way supplied the said drawings, specifications, or other data, is not to be regarded by implication or otherwise as in any manner licensing the holder or any other person or corporation, or conveying any rights or permission to manufacture, use, or sell any patented invention that may in any way be related thereto.

REPORT DOCUMENTATION PAGE		READ INSTRUCTIONS BEFORE COMPLETING FORM
1. REPORT NUMBER	2. GOVT ACCESSION NO.	3. RECIPIENT'S CATALOG NUMBER
	AD-A096600	
4. TITLE (and Subtitle)	5. TYPE OF REPORT & PERIOD COVERED	
(6) GTD Analysis of a Strip Scatterer in the Near Field of an Antenna.	(9) Technical Report.	
	6. PERFORMING ORG. REPORT NUMBER	
	(14) ESL-713303-1	
7. AUTHOR(s)	8. CONTRACT OR GRANT NUMBER(s)	
(10) Yueh-Chi/Chang	(15) Contract N62269-80-C-0384	
9. PERFORMING ORGANIZATION NAME AND ADDRESS	10. PROGRAM ELEMENT, PROJECT, TASK AREA & WORK UNIT NUMBERS	
The Ohio State University ElectroScience Laboratory, Department of Electrical Engineering, Columbus, Ohio 43212	Project N62269-80-32-01618	
11. CONTROLLING OFFICE NAME AND ADDRESS	12. REPORT DATE	
Department of the Navy Naval Air Development Center Warminster, PA 18974	(11) December 1980	
14. MONITORING AGENCY NAME & ADDRESS (if different from Controlling Office)	13. NUMBER OF PAGES	
(12) 103	97	
	15. SECURITY CLASS. (of this report)	
	Unclassified	
	15a. DECLASSIFICATION/DOWNGRADING SCHEDULE	
16. DISTRIBUTION STATEMENT (of this Report)		
This document has been approved for public release and sale; its distribution is unlimited.		
17. DISTRIBUTION STATEMENT (of the abstract entered in Block 20, if different from Report)		
18. SUPPLEMENTARY NOTES		
19. KEY WORDS (Continue on reverse side if necessary and identify by block number)		
Antenna Far field pattern Scattering Geometrical Theory of Diffraction	Slope diffraction Aperture integration	
20. ABSTRACT (Continue on reverse side if necessary and identify by block number)		
Various computer codes have been developed by using Geometrical Theory of Diffraction (GTD) to calculate the scattering effects associated with antennas in the presence of scattering structures. These codes are most useful for low gain antennas although they can simulate large antennas using the superposition principle. Unfortunately, this approach results in large computer run times for antennas that have to be subdivided into many smaller elements. Two approaches for overcoming this limitation in two-dimensional		

402251

20. cases are investigated in this thesis: a) the large subaperture technique and b) the two-point GTD source field method. Both approaches use the GTD method to calculate the scattering from structures in a similar way to that used in the present codes. However, the fields of the antennas or sources are treated in ways to permit more efficient calculations in these approaches. Both approaches have turned out to be useful and complement each other.

Accession For	
NTIS GRA&I	<input checked="" type="checkbox"/>
DTIC TAB	<input type="checkbox"/>
Unannounced	<input type="checkbox"/>
Justification <i>None on file</i>	
For	
Distribution/	
Availability Codes	
Dist	Avail and/or Special
<i>A</i>	

## CONTENTS

Chapter		Page
I	INTRODUCTION.....	1
II	BASIC GTD THEORY.....	4
	A. Geometrical-Optics Field	5
	B. Ordinary Edge Diffraction	6
	1. The wedge	6
	2. The half plane	9
	C. Slope Diffraction	9
III	APERTURE INTEGRATION SOURCE AND GTD SCATTERING...	14
	A. Source Field Without the Scatterer	16
	B. Total Field with the Strip Scatterer Present	17
	1. Source field with the scatterer present	17
	2. Reflected field from the strip	18
	3. Diffracted field from the edges of the scatterer	20
	4. Total far field	22
IV	LARGE SUBAPERTURE TECHNIQUE.....	23
	A. Source Field with the Scatterer Present	24
	B. Reflected Field from the Strip	25
	C. Diffracted Field	26
V	TWO-POINT GTD SOURCE FIELD METHOD	28
	A. Uniform Source Distribution	28
	1. Source field without scattered	28
	a. Near field	28
	b. Far field	30
	2. With the strip scatterer present	31
	a. Source field with scatterer present	33
	b. Reflection from the scatterer	33
	c. Diffraction from the scatterer	35

	B.	Source Distribution with Zero Edge Illumination	38
		1. Source field without the scatterer	38
		2. Total solution with the strip scatterer present	40
		a. Source field with the scatterer	41
		b. The reflected field	41
		c. The diffracted field	42
VI		SLOPE DIFFRACTION FROM THE SCATTERER.....	43
VII		RESULTS AND DISCUSSIONS.....	45
	A.	Large Subaperture Technique	46
		1. Type 1 - Uniform source distribution	46
		2. Type 2 - Cosine distribution	46
	B.	Two-point GTD Source Field Method	57
	C.	Slope Diffraction from the Scatterer	65
	D.	Combination of Large Subaperture and Two-point GTD Source Methods	71
VIII		EXAMPLES OF OTHER APPLICATIONS.....	80
	A.	Scanning Mode	80
	B.	Cylindrical Wave Radiator	83
		1. Terms Caused by Geometric Optics Source	84
		2. Terms Caused by Diffraction Sources	84
IX		CONCLUSIONS.....	90
Appendix			
	A	ELEMENT PATTERN USED FOR APERTURE INTEGRATION....	92
		REFERENCES.....	96

## CHAPTER I

### INTRODUCTION

In order to investigate the scattering effects associated with antennas in the presence of scattering structures, two computer codes have been developed: The Aircraft Antenna Code [1] and The Basic Scattering Code [2]. The scattering structures associated with these codes are modeled by finite flat plates and cylinders, e.g., the wings or tail structures of an aircraft can be modeled by plates and the fuselage by a cylinder. Both codes use geometrical theory of diffraction (GTD) to analyze the scattering effects, which are most useful for low gain antennas although they can simulate large antennas using the superposition principle. Thus scattered fields can be calculated by superimposing the contribution from each element. Unfortunately, this approach results in large computer run times for antennas that have to be subdivided into many smaller elements.

Two approaches for overcoming this limitation are investigated in this thesis: a) the large subaperture technique and b) the two-point GTD source field method. Both approaches use the GTD method to calculate the scattering from structures in a manner similar to that used in the present codes[1,2]; however, the fields of the antennas or sources are treated in a way to permit more efficient calculations of these approaches. Both approaches are useful and com-

plement each other. For the purpose of review, the basic GTD theory is presented briefly in Chapter II and a two-dimensional model of the existing computer codes is discussed in Chapter III.

The first approach is discussed in Chapter IV which uses large subapertures to represent the large antenna aperture distribution. Basically, it calculates the antenna fields in the same way as the aperture integration (AI) method except that elements are grouped into large subapertures. This method works well in most regions if the large subapertures are no larger than one wavelength. Otherwise, it only works well in some regions, especially near the main beam.

In the second approach, which is discussed in Chapter V, GTD provides a very efficient method because the antenna fields can be modeled by a 2-point edge diffraction technique in the regions sufficiently removed from the main beam. However, GTD can not be used to calculate the antenna fields in the main beam since one loses some information about the aperture distribution between the two edges of the antenna.

In the two-point GTD source field approach, the sources of the incident fields on the strip scatterer are located at each edge of the antenna. When a strip scatterer is near the projected aperture of the antenna, the incident field from the source at the nearest edge has a large slope. Thus ordinary edge diffractions from the scatterer become insufficient to get a good result. So, slope diffraction from the scatterer was added to partially solve the problem as discussed in Chapter VI. However, when a strip is very close to

a shadow boundary of the projected aperture, the incident field from the edge source is too complicated to model by a uniform wave plus a slope wave. Consequently, the large subaperture approach must be used for these cases.

The results and discussions are presented in Chapter VII to show the efficiency and limitations of the two approaches. Finally, two specific examples are demonstrated in Chapter VIII so that the reader can relate this study to practical application.

In this thesis, only the two-dimensional (2-D) case is investigated in that it provides insight for the problem without adding the unnecessary complexities associated with the three-dimensional (3-D) case. For the 3-D case, some more complicated factors such as geometry, polarization, and corner diffraction must be considered.

## CHAPTER II

### BASIC GTD THEORY

The basic GTD solutions of the two-dimensional case are reviewed in this chapter, and these solutions are applied to solve fields in the following chapters. When a wedge is illuminated by a line source, GTD is used to analyze the radiation from the source and the scattering from the wedge. For the geometry shown in Figure 1, the total field caused by the line source in the presence of the wedge is expressed by

$$E^t = E^s + E^r + E^d \quad (2-1)$$

The source field  $E^s$  is the electric field radiated directly from the source, the reflected field  $E^r$  is the electric field reflected from the surface of the wedge, and the superposition of these two fields is called geometrical-optics field. The diffracted field  $E^d$  from the edge of the wedge includes ordinary edge diffraction  $E_0^d$ , and slope diffraction  $E_s^d$ . For most cases, first order diffraction is enough to solve the scattering problem, but in some cases, slope diffraction must be added to the solutions.

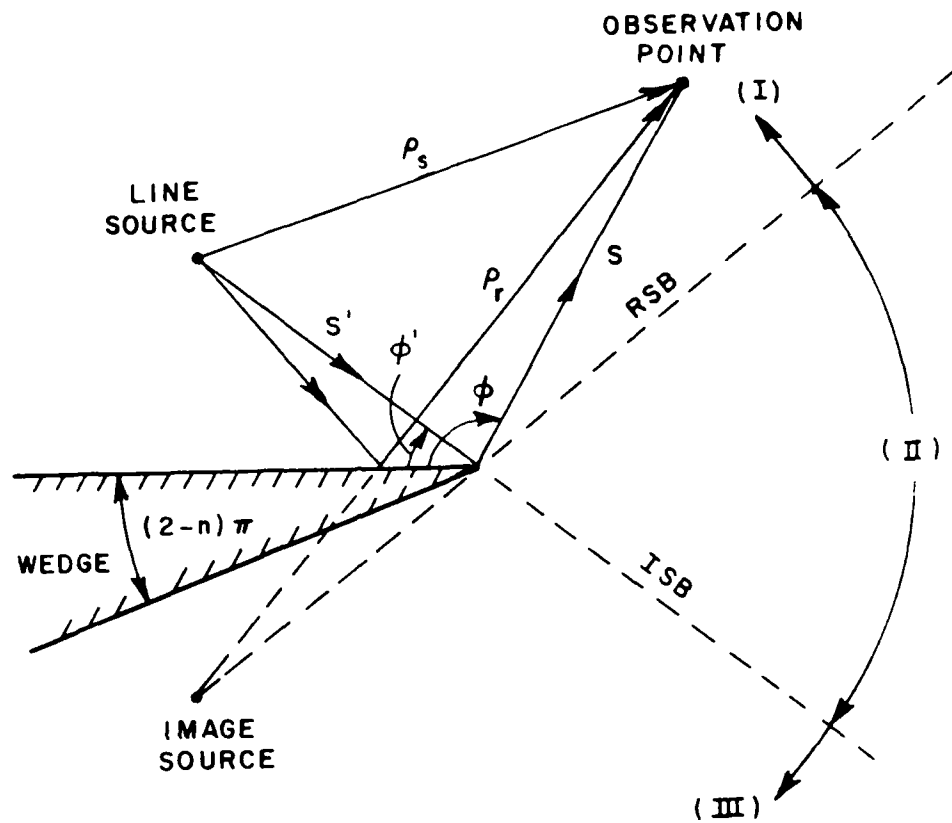


Figure 1. Geometry for two-dimensional wedge diffraction.

A. Geometrical-Optics Field

As shown in Figure 1, the incident shadow boundary (ISB) is determined by the locations of the line source and the edge, and reflection shadow-boundary (RSB) is determined by the image source and the edge. Once these boundaries have been defined, the source field  $E^S$  can be expressed by

$$E^S = \begin{cases} \frac{e^{-jk\rho_s}}{\sqrt{\rho_s}} & \text{for } 0 < \phi < 180^\circ + \phi' \\ 0 & \text{elsewhere} \end{cases} \quad (2-2)$$

That is, the source field exists in regions I and II as shown in Figure 1. Similarly, the reflected field  $E^r$  can be expressed by

$$E^r = \begin{cases} \mp \frac{e^{-jk\rho_r}}{\sqrt{\rho_r}} & \text{for } 0 < \phi < 180^\circ - \phi' \\ 0 & \text{elsewhere} \end{cases} \quad (2-3)$$

which exists in region I only. Note that  $\rho_r$  is the distance from the image source to observation point and one uses the minus sign for the TE case and plus sign for the TM case.

## B. Ordinary Edge Diffraction

### 1. The wedge

The ordinary diffracted field at the observation point  $(s, \phi)$  is given by [3]

$$E_0^d = E^I(Q_E) \cdot D_{s,h}(L; \phi, \phi', n) \frac{e^{-jks}}{\sqrt{s}} \quad (2-4)$$

where  $E^I(Q_E)$  is the incident field from the line source at the edge  $Q_E$ , which can be expressed by

$$E^I(Q_E) = \frac{e^{-jks'}}{\sqrt{s'}} \quad (2-5)$$

Note that  $s'$  and  $s$  are the distances between the edge and the source and the observation point, respectively. The phase factor is  $e^{-jks}$  and  $1/\sqrt{s}$  is the 2-D spreading factor. The diffraction coefficients  $D_S$  and  $D_h$  are given by

$$D_S(L; \phi, \phi', n) = D_I(L; \phi - \phi', n) \mp D_I(L; \phi + \phi', n) \quad (2-6)$$

where the minus (-) sign applies for  $D_S$ , which corresponds to the TE case, and plus (+) sign applies for  $D_h$ , which corresponds to the TM case. Note that  $D_I$  is given by

$$D_I(L; \beta, n) = \frac{-e^{-j\frac{\pi}{4}}}{2n\sqrt{2\pi k}} \left[ \cot\left(\frac{\pi+\beta}{2n}\right) F(kLa^+(\beta)) + \cot\left(\frac{\pi-\beta}{2n}\right) F(kLa^-(\beta)) \right], \quad (2-7)$$

where  $\beta = \phi - \phi'$  and  $n = 2 - \frac{WA}{\pi}$ ,

with wedge angle  $WA$  given in radians. The term  $a^\pm(\beta)$  is a measure of the angular separation between the observation point and the incident or reflection shadow boundary and is expressed by

$$a^{\pm}(\beta) = 2 \cos^2\left(\frac{2\pi n N^{\pm} - \beta}{2}\right), \quad (2-8)$$

where  $N^{\pm}$  are integers which most nearly satisfy the equations

$$2\pi n N^+ - \beta = \pi, \quad (2-9)$$

and

$$2\pi n N^- - \beta = -\pi \quad (2-10)$$

The distance parameter  $L$  is given by

$$L = \frac{ss'}{s+s'}, \quad (2-11)$$

and the transition function  $F(x)$  is basically a Fresnel integral, which is given by

$$F(x) = 2j\sqrt{x} e^{jx} \int_{\sqrt{x}}^{\infty} e^{-j\tau^2} d\tau \quad (2-12)$$

where  $X = kLa^{\pm}(\beta)$

If the line source is far away from the edge, that is, in the case of  $s' \rightarrow \infty$ , the incident field becomes a plane wave. In that case, the distance parameter  $L \rightarrow s$ .

## 2. The half plane

When  $n=2$ , the wedge becomes a half plane and the diffraction coefficients  $D_s$  and  $D_h$  can be simplified to

$$D_{\frac{s}{h}}(L; \phi, \phi') = D_I(L; \phi - \phi') \mp D_I(L; \phi + \phi') \quad (2-13)$$

In which  $D_I$  are expressed by

$$D_I(L; \beta) = \frac{-e^{-j\frac{\pi}{4}}}{2\sqrt{2\pi k}} \frac{F[kLa(\beta)]}{\cos \frac{\beta}{2}} \quad (2-14)$$

and  $a(\beta)$  is simply given by

$$a(\beta) = 2 \cos^2 \frac{\beta}{2} \quad (2-15)$$

### C. Slope Diffraction

When there is zero incident field on the edge or the slope of the incident wave is large, slope diffraction becomes significant. This section derives the equations for the slope diffraction, which has a form similar to ordinary edge diffraction except that the slope diffraction coefficients  $\partial D_{s,h} / \partial \phi'$  and the slope of the incident field at the edge  $\partial E^I(Q_E) / \partial n$  are used.

Slope diffraction for a cylindrical wave can be derived from edge diffraction by considering a line dipole source composed of two line sources [4] as shown in Figure 2. The field of this dipole source is given by

$$E^I = I \cdot \frac{e^{-jks_+}}{s_+} - I \cdot \frac{e^{-jks_-}}{s_-}, \quad (2-16)$$

where  $s_+$  and  $s_-$  are the respective distances from each line source to the field point. For small spacings  $l \ll s'$ , one obtains

$$s_{\pm} = s' \mp \frac{1}{2} l \sin \psi \quad (2-17)$$

where the angle  $\psi$  is shown in Figure 2. Thus, the source field can be expressed as

$$\begin{aligned} E^I &= I \cdot \frac{e^{-jks'}}{\sqrt{s'}} \left[ e^{j\frac{kl}{2} \sin \psi} - e^{-j\frac{kl}{2} \sin \psi} \right] \\ &= 2jI \sin \left( \frac{kl}{2} \sin \psi \right) \frac{e^{-jks'}}{\sqrt{s'}} \end{aligned} \quad (2-18)$$

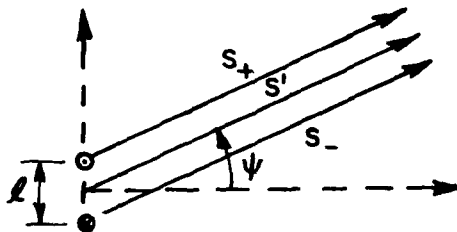


Figure 2. A line dipole source for slope diffraction.

For a slope diffraction source  $kl \rightarrow 0$ , and

$$E^I = jkI\ell \sin\psi \frac{e^{-jks'}}{\sqrt{s'}} \quad (2-19)$$

The slope diffraction field can be derived by superimposing the diffracted fields from the two line sources as shown in Figure 3.

Thus using Equations (2-4), one finds

$$E_s^d = I \frac{e^{-jks'}}{s'} \left[ D_{s,h}(L; \phi, \phi' + \frac{\Delta\phi'}{2}) - D_{s,h}(L; \phi, \phi' - \frac{\Delta\phi'}{2}) \right] \cdot \frac{e^{-jks}}{s} \quad (2-20)$$

Since  $\Delta\phi' \rightarrow 0$  as  $l \ll s'$ , Equation (2-20) can be expressed as

$$E_s^d = I \frac{e^{-jks'}}{\sqrt{s'}} \frac{\partial D_{s,h}}{\partial \phi'} \Delta\phi' \frac{e^{-jks}}{\sqrt{s}} \quad (2-21)$$

Let  $n$  be the distance normal to the edge and normal to the incident ray from the source as shown in Figure 4. Note that  $n \rightarrow s' \cdot (\pi - \psi)$  as  $\psi \rightarrow \pi$ . Then the slope of the incident field at the edge can be expressed in terms of the distance  $n$  as follows:

$$\frac{\partial E^I}{\partial n} \Big|_{\eta_E} = \frac{-1}{s'} \frac{\partial E^I}{\partial \psi} \Big|_{\pi} = \frac{jkI\ell}{s'} \frac{e^{-jks'}}{\sqrt{s'}} \quad (2-22)$$

Since  $l = s' \Delta\phi'$ , Equation (2-22) can be expressed as

$$I \Delta\phi' \frac{e^{-jks'}}{\sqrt{s'}} = \frac{1}{jk} \frac{\partial E^I}{\partial n} \Big|_{\eta_E} \quad (2-23)$$

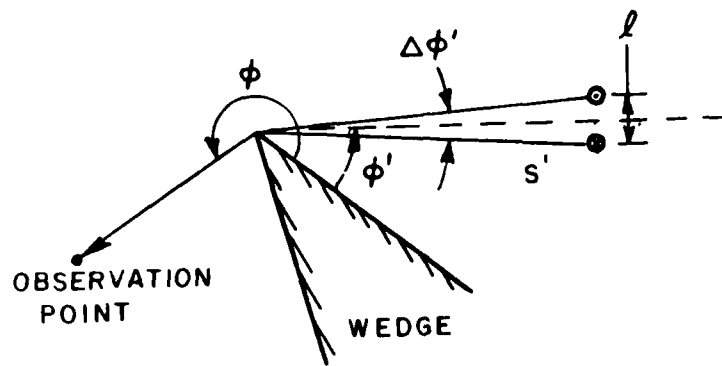


Figure 3. 2-D slope diffraction for a wedge.

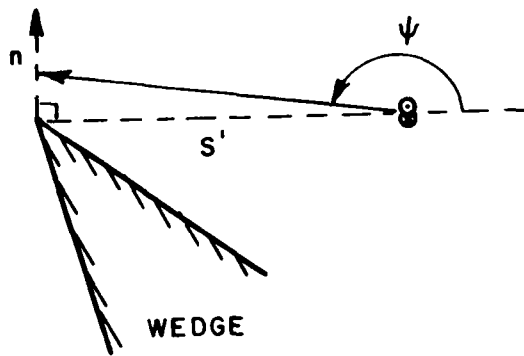


Figure 4. Normal vector  $n$  of the incident field for slope diffraction.

Combining Equations (2-21) and (2-23), one gets

$$E_s^d = \frac{1}{jk} \left. \frac{\partial E^I}{\partial n} \right|_0 \cdot \frac{\partial D_{s,h}}{\partial \phi'} \frac{e^{-jks}}{\sqrt{s}} \quad (2-24)$$

The slope diffraction coefficient  $\partial D_{s,h} / \partial \phi'$  can be expressed by

$$\frac{\partial D_{s,h}}{\partial \phi'} = D_{pI}(L; \phi - \phi') \pm D_{pI}(L; \phi + \phi') \quad (2-25)$$

where  $D_{pI}(L; \beta) = \frac{\partial D_I(L; \beta)}{\partial \phi'} \quad (2-26)$

Note that the plus sign is used for the TE case and minus sign for the TM case, and  $D_I$  is defined in Equation (2-14).

CHAPTER III  
APERTURE INTEGRATION SOURCE AND GTD SCATTERING

The original method used to solve a 2-D scattering problem is studied in this chapter. The total scattered fields are calculated in the same manner as the existing codes [1,2] for the purpose of reference and comparison. Figure 5 shows the 2-D model which is analyzed in the following chapters. A source antenna of width  $L$  is located between edge points  $Q_{s1}(x_{s1}, y_{s1})$  and  $Q_{s2}(x_{s2}, y_{s2})$  and a strip with edge points  $Q_{c1}(x_{c1}, y_{c1})$  and  $Q_{c2}(x_{c2}, y_{c2})$  represents a perfectly conducting scatterer. Then the total field of the antenna with the strip pattern present is composed of the source, the reflected, and the diffracted fields, which are calculated separately.

The fields scattered from the strip are calculated for each element, that is, each element of the antenna aperture distribution is taken as a source for the diffracted fields as shown in Figure 6. Then the contributions from each element are superimposed to obtain the total field. This method gives accurate results, but is not efficient for large antennas. Two methods for improving the efficiency are discussed in Chapters IV and V.

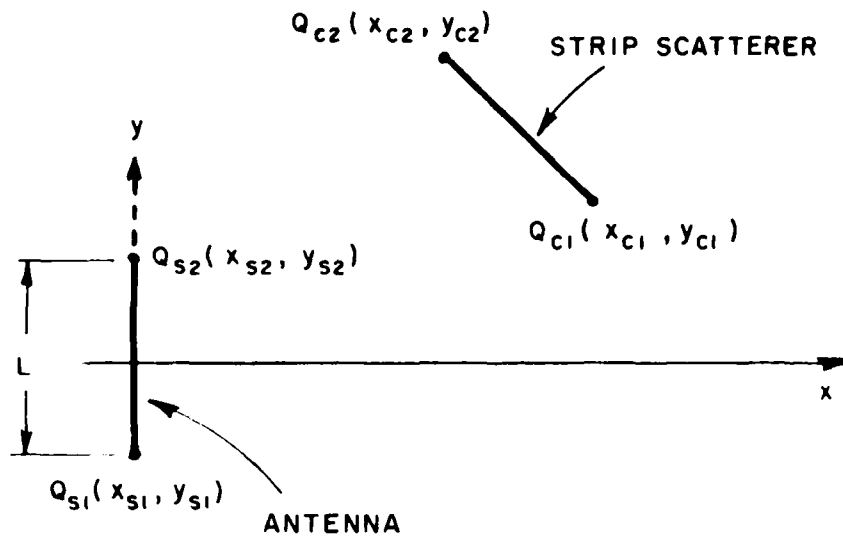


Figure 5. A 2-D model of a scattering problem.

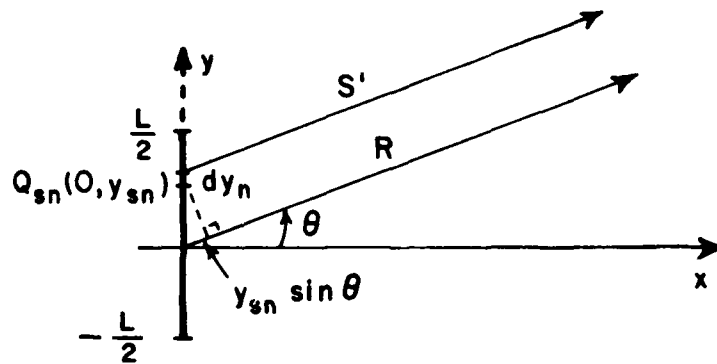


Figure 6. The far field approximation for the antenna.

### A. Source Field Without the Scatterer

Consider the fields of the antenna without the scatterer first. Using the aperture integration, the antenna is divided into  $N$  small elements. For the  $n$ th element  $dy_n$  located at  $Q_{sn}(0, y_{sn})$  as shown in Figure 6, the field contribution  $dE_n^S$  is given by

$$dE_n^S = \frac{A(y_{sn})e^{-jks'}}{\sqrt{s'}} dy_n \cdot \cos \frac{\theta}{2} \quad (3-1)$$

where  $A(y)$  is the aperture distribution and a  $\cos \frac{\theta}{2}$  element pattern gives the most appropriate modeling for an edge as derived in Appendix A. This approach provides excellent overlapping of GTD and AI for the analysis of reflector antennas [5,6]. Since  $s' = R - y_{sn} \sin \theta$  for the far field, one finds

$$dE_n^S = A(y_{sn}) e^{jky_{sn} \sin \theta} dy_n \cdot \cos \frac{\theta}{2} \cdot \frac{e^{-jkR}}{\sqrt{R}} \quad (3-2)$$

So the total far field pattern function  $F(\theta)$  is obtained by superposing all the contributions from the  $N$  elements, such that

$$F(\theta) = \sum_{n=1}^N A(y_{sn}) e^{jky_{sn} \sin \theta} \Delta y \cos \frac{\theta}{2} \quad (3-3)$$

where  $\Delta y = L/N$

and  $y_{sn} = -\frac{L}{2} + \frac{\Delta y}{2} + (n-1)\Delta y$ .

B. Total Field with the Strip Scatterer Present

Next, consider the antenna in the presence of the strip scatterer as shown in Figure 7. Let  $\theta_{nj}^s$  represent the angle and  $s_{nj}$  represent the distance from  $Q_{sn}$  to  $Q_{cj}$ , respectively, where  $n = 1, 2, \dots, N$  and  $j=1,2$ .  $\theta_{n1}^s$  and  $\theta_{n2}^s$  correspond to the shadow boundaries of the  $n$ th element at  $Q_{sn}$ . Then the source, the reflected and the diffracted fields can be analyzed as follows.

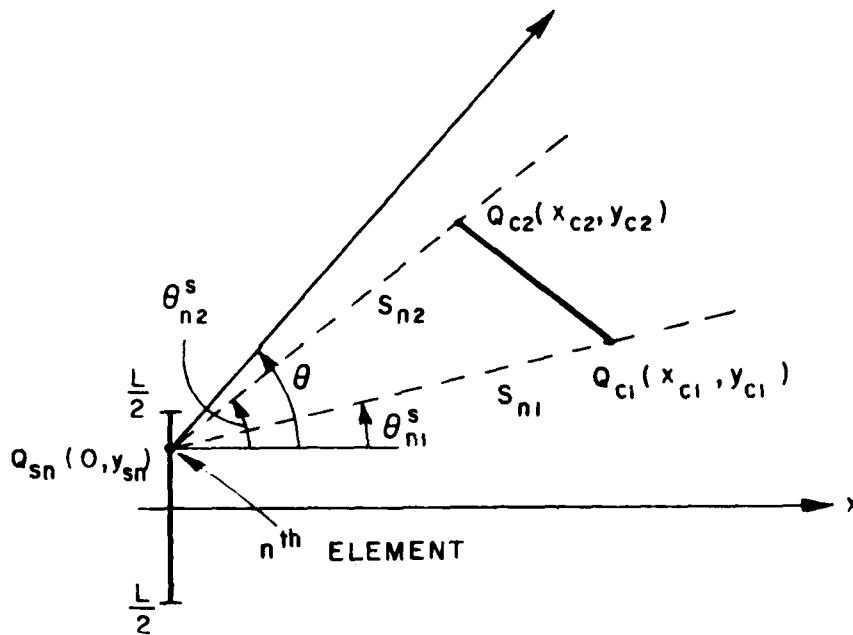


Figure 7. The source field and its shadow boundaries of the  $n$ th element.

1. Source field with the scatterer present

Since some of the source fields are blocked by the strip scatterer, it can be seen from Figure 7 that the pattern function of the source field from element  $Q_{sn}$  can be represented by

$$F_n^S(\theta) = \begin{cases} 0 & \text{for } \theta_{n1}^S < \theta < \theta_{n2}^S, \text{ and} \\ A(y_{sn}) e^{jky_{sn} \sin \theta} \Delta y & \text{elsewhere} \end{cases} \quad (3-4)$$

By superposition, the total source field pattern is given by

$$F^S(\theta) = \sum_{n=1}^N F_n^S(\theta) \quad (3-5)$$

Note that each source element has its corresponding shadow boundary angles at  $\theta_{n1}^S$  and  $\theta_{n2}^S$ .

## 2. Reflected field from the strip

At the same time, there are some fields reflected by the scatterer. The image method is used to calculate the reflected fields. As shown in Figure 8, the  $n$ th image element is located at  $Q_{In}(x_{In}, y_{In})$  and its contribution to the reflected field is given by

$$F_n^R(\theta) = \begin{cases} \mp A(y_{sn}) e^{j\psi_{In}} \Delta y & \text{for } \theta_{n2}^R < \theta < \theta_{n1}^R, \text{ and} \\ 0 & \text{elsewhere} \end{cases} \quad (3-6)$$

where the sign is defined in Equation (2-3) and  $\psi_{In} = k(x_{In} \cos \theta + y_{In} \sin \theta)$  refers the phase to the origin (0,0). The shadow boundary angles are  $\theta_{n1}^R$  and  $\theta_{n2}^R$  of the image point  $Q_{In}$ . Then, the total pattern of the reflected field is given by

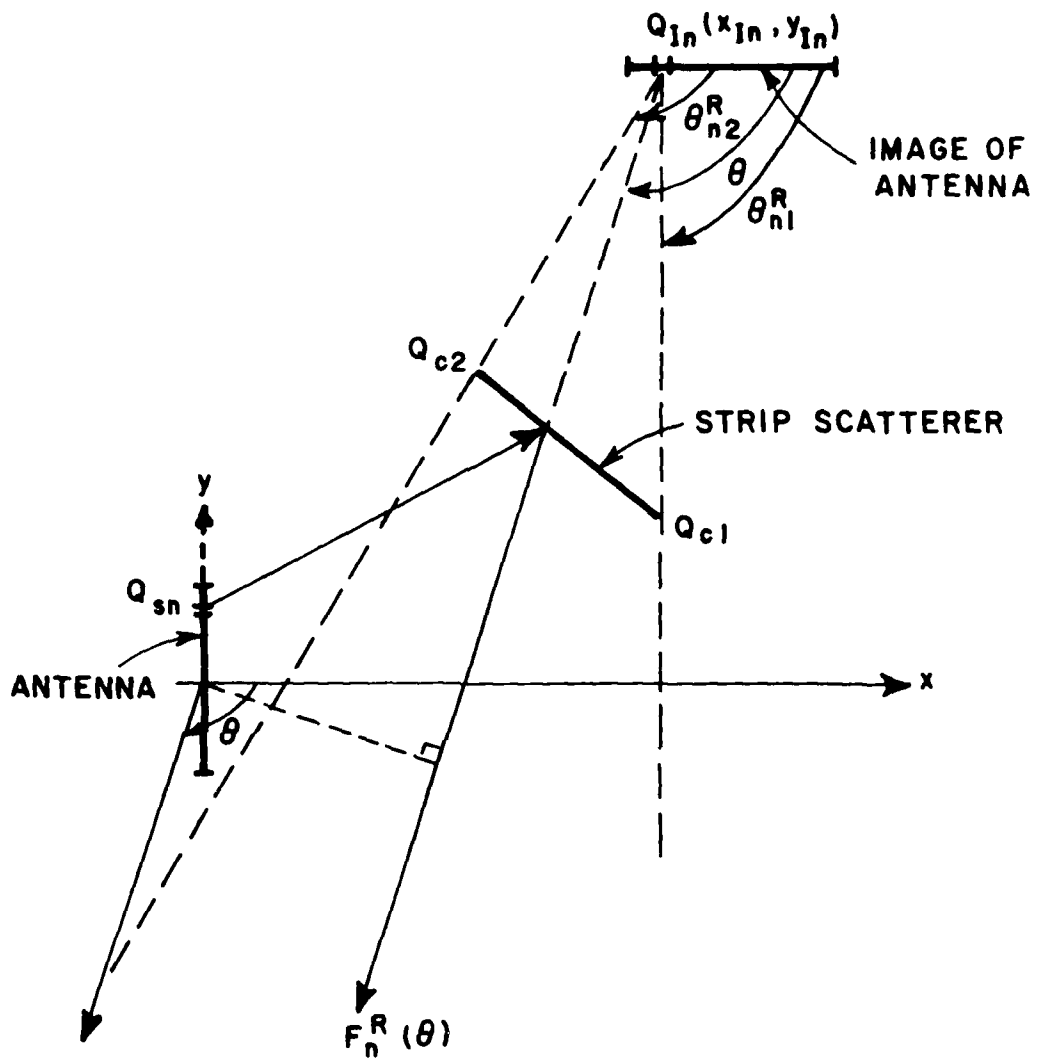


Figure 8. The reflected field and its shadow boundaries.

$$F^R(\theta) = \sum_{n=1}^N F_n^R(\theta) \quad (3-7)$$

### 3. Diffracted field from the edges of the scatterer

Next, the diffracted fields from the two edges of the scatterer are evaluated. For the  $n$ th source element  $Q_{sn}$ , there are two diffracted fields,  $E_{n1}^d(\theta)$  and  $E_{n2}^d(\theta)$ , from the two edges of the scatterer, respectively, as shown in Figure 9. The far field pattern  $F_{nj}^d(\theta)$  of the diffracted field from  $Q_{cj}$  as caused by the  $n$ th source element is given by

$$F_{nj}^d(\theta) = E_{nj}^I(Q_{ij}) \cdot D_{nj} \cdot \frac{e^{jks_j}}{\sqrt{s_j}} \quad n=1,2\dots N, j=1,2 \quad (3-8)$$

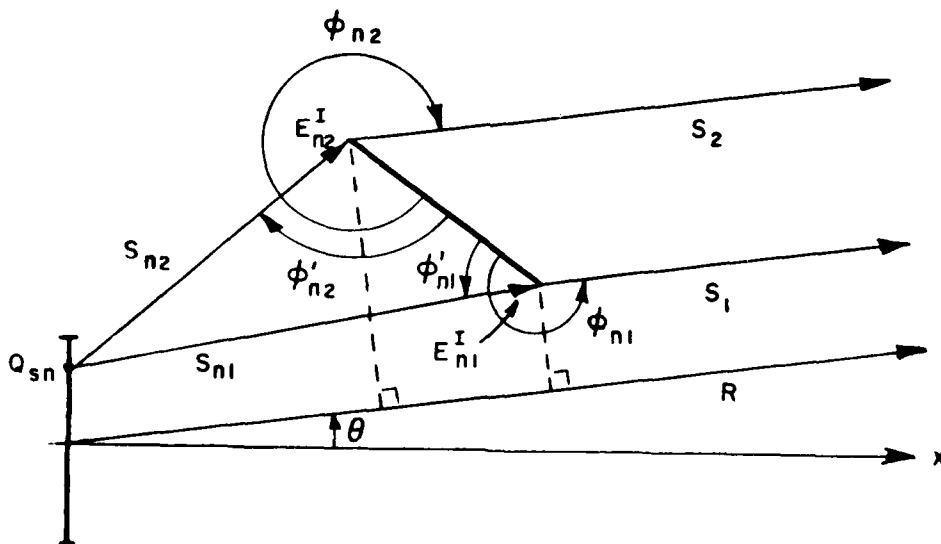


Figure 9. The geometry for the diffracted fields.

where the incident field  $E_{nj}^I$  from  $Q_{sn}$  to  $Q_{cj}$  is given by

$$E_{nj}^I(Q_{cj}) = A(y_{sn}) \frac{e^{-jks_{nj}}}{\sqrt{s_{nj}}} \cos \frac{\theta}{2} \quad (3-9)$$

and  $D_{nj}$  is the diffraction coefficient which is given by

$$D_{nj} = D_I(L_{nj}; \phi_{nj} - \phi'_{nj}) \mp D_I(L_{nj}; \phi_{nj} + \phi'_{nj}) \quad (3-10)$$

where

$D_I(L; \phi - \phi')$  was defined in Equation (2-14).

Note that one should use the "-" sign for the TE case, and the "+" sign for the TM case. Further,

$$L_{nj} = \frac{s_{nj} \cdot s_j}{s_{nj} + s_j} \rightarrow s_{nj} \text{ as } s_j \rightarrow \infty$$

and

$$s_j = R - (x_{cj} \cos \theta + y_{cj} \sin \theta)$$

So the total pattern function associated with all the first order edge diffracted fields is given by summing all the diffracted fields from the  $N$  elements, such that

$$F^d(\theta) = \sum_{n=1}^N \sum_{j=1}^2 E_{nj}^I(Q_{cj}) \cdot D_{nj} e^{jk\psi_{dj}} \quad (3-11)$$

where

$$\psi_{dj} = k(x_{cj} \cos\theta + y_{cj} \sin\theta). \quad (3-12)$$

#### 4. Total far field

Recall that the far field pattern of the antenna with the strip scatterer present is given by superimposing the source, reflected, and diffracted fields as stated in equation (2-1). Thus,

$$F^{\text{tot}}(\theta) = F^S(\theta) + F^R(\theta) + F^d(\theta).$$

## CHAPTER IV

### LARGE SUBAPERTURE TECHNIQUE

When an antenna or source aperture is quite large, it takes a lot of computer run time if one uses the method discussed in the last chapter. Most of the time is spent evaluating the diffracted fields for each little source element. For better efficiency, the large subaperture technique groups the source into equal size subapertures. The contribution of each subaperture to the diffracted field is obtained by using the subaperture as a single source. In other words, its incident field on the edges of the scatterer is the sum of the contributions from all the little elements within the larger limits of the subaperture; these contributions are calculated in the same way as done in the previous chapter. Then, the mid-point of each subaperture is used to evaluate the diffraction coefficient for that subaperture. This approximation works well as long as the subapertures are not too large.

The source and the reflected fields are grouped with the diffracted fields so that the total field is continuous across the shadow boundaries. This will be shown by computer plots given in Chapter VII. The analyses of the source, reflected, and diffracted fields are similar to those in Chapter III and given in the following sections.

A. Source Field with the Scatterer Present

In this approach, each subaperture which includes several elements is considered as an individual source. Let  $M$  be the number of little radiators within the subaperture limits. The source field pattern of the  $k$ th subaperture is, then, given by

$$F_k^S(\theta) = \begin{cases} 0 & \text{for } \theta_{k1} < \theta < \theta_{k2}, \text{ and} \\ \sum_{m=1}^M A(y_{km}) e^{jky_{km} \sin \theta} \cdot \Delta y & \text{elsewhere,} \end{cases} \quad (4-1)$$

where  $y_{km}$  represents the location of the  $m$ th element in the  $k$ th subaperture, and  $\theta_{k1}$ ,  $\theta_{k2}$  are the shadow boundary angles which are determined by the mid-point  $(0, y_k)$  of the  $k$ th subaperture as shown in Figure 10.

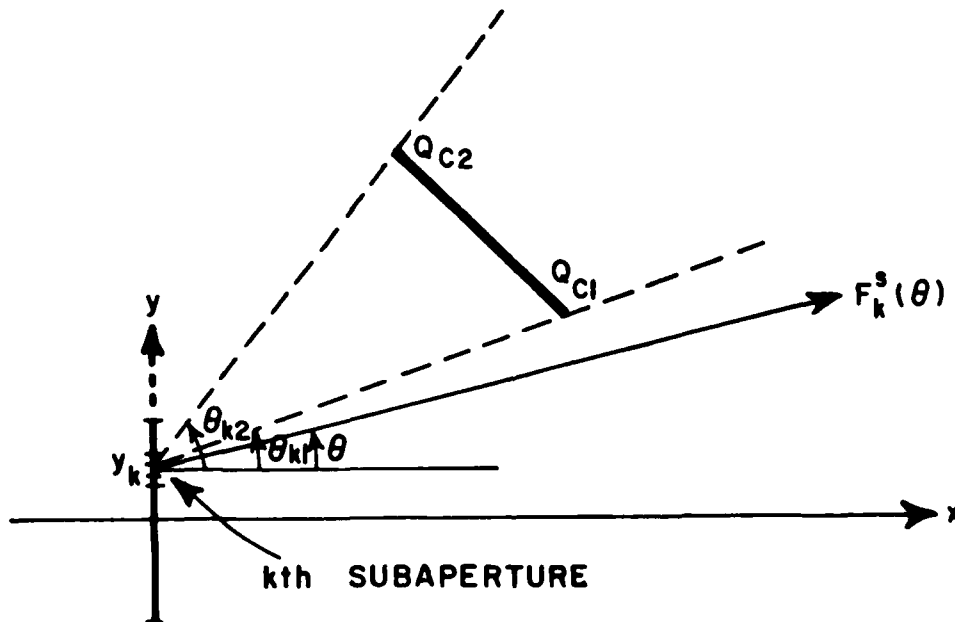


Figure 10. The source field and its shadow boundaries for the  $k$ th subaperture.

Then, the total source field is the superposition of the source fields of all subapertures as given by

$$F^S(\theta) = \sum_{k=1}^K F_k^S(\theta), \quad (4-2)$$

where K is the number of subapertures.

#### B. Reflected Field from the Strip

The reflected fields are grouped in the same way as the source fields and can be expressed by

$$F^R(\theta) = \sum_{k=1}^K F_k^R(\theta), \quad (4-3)$$

where

$$F_k^R(\theta) = \begin{cases} \sum_{m=1}^M A(y_{km}) e^{j\psi_{km}^I} \cdot \Delta y & \text{for } \theta_{k1}^R < \theta < \theta_{k2}^R, \text{ and} \\ 0 & \text{elsewhere,} \end{cases} \quad (4-4)$$

and

$$\psi_{km}^I = k(x_{km}^I \cos \theta + y_{km}^I \sin \theta),$$

with  $(x_{km}^I, y_{km}^I)$  being the coordinates of the image point for the source point  $(0, y_{km})$ . Note that  $\theta_{k1}^R$  and  $\theta_{k2}^R$  are the shadow boundary angles of the reflected field for the  $k$ th subaperture.

### C. Diffraction Field

As previously discussed, the incident field  $E_{kj}^I$  on the edge  $Q_{cj}$  of the strip scatterer from the  $k$ th subaperture is the sum of all the contributions from  $M$  elements in this subaperture. That is

$$E_{kj}^I = \sum_{m=1}^M A(y_{km}) \frac{e^{-jks_{kmj}}}{\sqrt{s_{kmj}}} \quad (4-5)$$

where  $s_{mkj}$  represents the distance from the source point  $(0, y_{km})$  to the diffracting edge  $Q_{cj}$ . Note that  $j=1$  or  $2$  indicates the two edges making up the strip. The diffraction coefficient  $D_{kj}$  for the  $k$ th subaperture may be expressed by

$$D_{kj} = D_I(s_{kj}; \phi_{kj} - \phi'_{kj}) \mp D_I(s_{kj}; \phi_{kj} + \phi'_{kj}) \quad (4-6)$$

where  $\phi_{kj}$ ,  $\phi'_{kj}$ , and  $s_{kj}$  are determined relative to the midpoint  $(0, y_k)$  of the subaperture and the appropriate edge, as shown in Figure 11.

So, the pattern of the diffracted field  $F^d(\theta)$  is given by

$$F^d(\theta) = \sum_{k=1}^K \sum_{j=1}^2 E_{kj}^I(\theta) \cdot D_{kj} e^{jk\psi_{dj}} \quad (4-7)$$

where  $\psi_{dj}$  is defined in Equation (3-12).

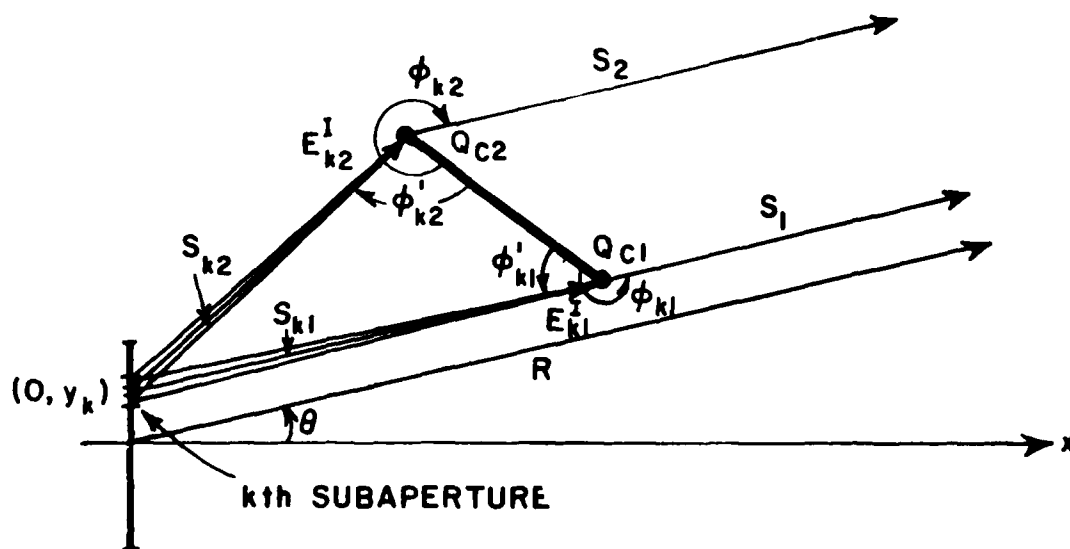


Figure 11. The diffracted fields of the  $k$ th subaperture.

CHAPTER V  
TWO-POINT GTD SOURCE FIELD METHOD

In this chapter, two types of source distribution are considered and analyzed by two different GTD approaches. The first one is a uniform source distribution on a source strip, which can be approximated by the diffracted fields from two edges of this strip illuminated by a uniform plane wave. The second one is a source distribution with zero edge illumination, e.g., a cosine distribution, which is analyzed in terms of the slope diffractions from two edges of the strip with the same illumination. Both approaches are more efficient than the aperture integration method as will be shown later.

A. Uniform Source Distribution

To start with, consider an antenna source with a uniform distribution. The procedure for analysis is about the same as that in Chapter III, but the source field is treated by a two-point GTD approach as described below.

1. Source field without scatterer

a. Near field

The near field of an aperture antenna as shown in Figure 5 can be analyzed by using GTD. In which case, the source field is approximated by the diffraction fields from the two edges of the antenna as shown in

Figure 12. Note that the diffracted fields are those of a conducting strip illuminated by an incident plane wave.

The diffracted field from each edge is given by

$$E_1^S(R, \theta) = E^i(Q_{s1}) \cdot D_{I1} \cdot \frac{e^{-jks_1}}{\sqrt{s_1}} \quad (5-1)$$

$$E_2^S(R, \theta) = E^i(Q_{s2}) \cdot D_{I2} \cdot \frac{e^{-jks_2}}{\sqrt{s_2}}$$

where  $E^i(Q_{s1}) = E^i(Q_{s2}) = E_0$

$$D_{I1} = D_I(s_1; \phi_1 + \phi_1') \quad (5-2)$$

$$D_{I2} = D_I(s_2; \phi_2 + \phi_2')$$

which are defined in Equation (2-16),  $\phi_1' = \phi_2' = \frac{\pi}{2}$ , and  $\phi_1, \phi_2, s_1$  and  $s_2$  are shown in Figure 12. Note that only  $D_I^+$  terms are used here which correspond to the reflected shadow boundaries in the  $z > 0$  half space. It has been shown that the  $D_I^+$  terms correspond to the physical optics or aperture integration fields [7].

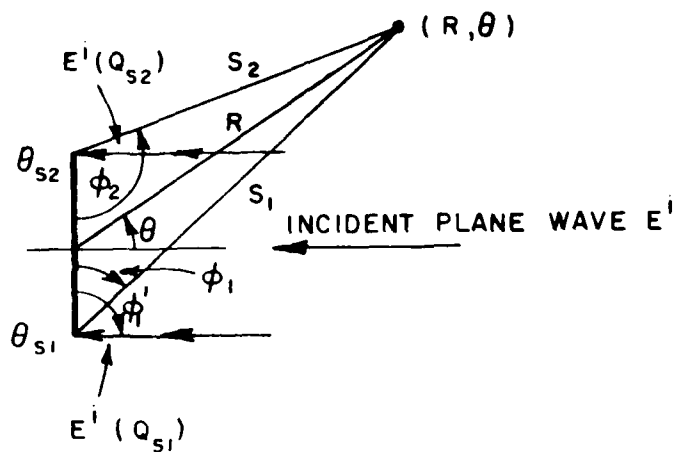


Figure 12. The near field of an antenna by using two-point GTD approach.

b. Far field

In the case of  $R \rightarrow \infty$ , as shown in Figure 13, the far field approximation is given by

$$\phi_1 = \frac{\pi}{2} - \theta ,$$

(5-3)

$$\phi_2 = \frac{\pi}{2} + \theta ,$$

$$s_1 = R - y_{s1} \sin \theta , \text{ and}$$

$$s_2 = R - y_{s2} \sin \theta .$$

(5-4)

So one obtains

$$E^S(R, \theta) = E^i(Q_{s1}) D_I(s_1; \pi - \theta) \frac{e^{-jks_1}}{\sqrt{s_1}} + E^i(Q_{s2}) D_I(s_2; \pi + \theta) \frac{e^{-jks_2}}{\sqrt{s_2}}, \quad (5-5)$$

where  $E^i(Q_{s1}) = E^i(Q_{s2}) = E_0$  in this case.

Then the far field pattern function  $F^S(\theta)$  is given by

$$F^S(\theta) = E_0 \left[ D_I(s_1; \pi - \theta) e^{jky_{s1} \sin \theta} + D_I(s_2; \pi + \theta) e^{jky_{s2} \sin \theta} \right] \quad (5-6)$$

as  $s_1, s_2 \rightarrow \infty$ .

## 2. With the strip scatterer present

The geometry of the antenna in the presence of the strip scatterer is shown in Figure 14. Let  $s_{ij}$  and  $\theta_{ij}^S$  represent the distance and the angle from  $Q_{si}$  to the scatterer edge  $Q_{cj}$  respectively, where  $i=1$  or  $2$  and  $j=1$  or  $2$ . It follows directly that

$$s_{ij} = \sqrt{(x_{cj} - x_{si})^2 + (y_{cj} - y_{si})^2}, \text{ and} \quad (5-7)$$

$$\theta_{ij}^S = \tan^{-1} \left( \frac{y_{cj} - y_{si}}{x_{cj} - x_{si}} \right). \quad (5-8)$$

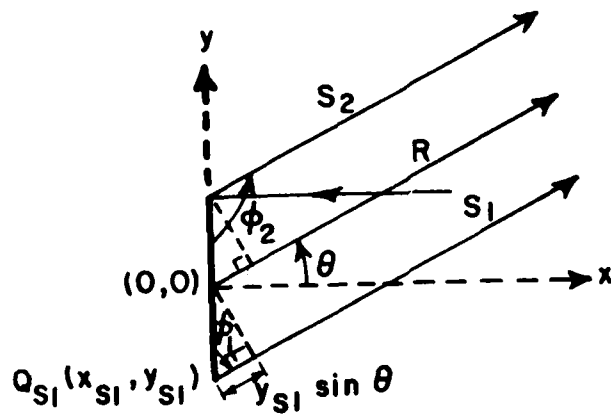


Figure 13. The far field of an antenna using two-point GTD approach.

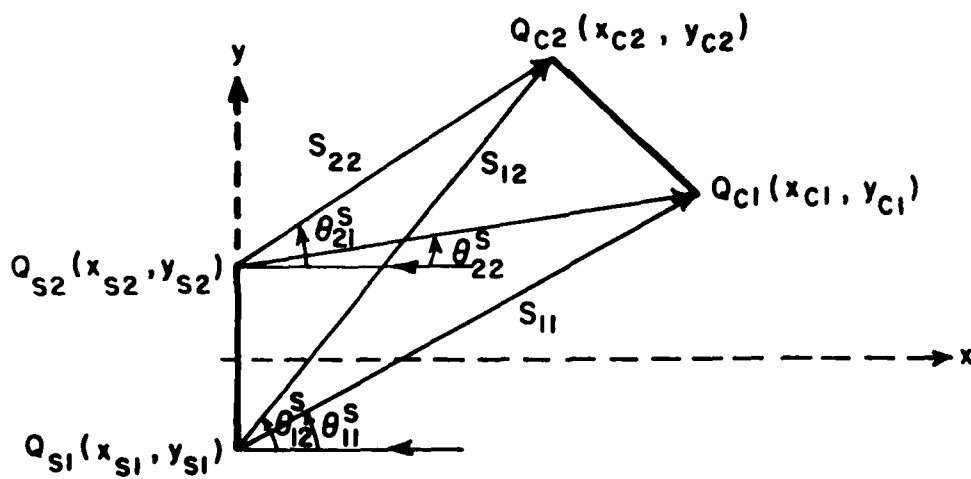


Figure 14. The geometry of the two-point GTD with the scatterer present.

a. Source field with scatterer present

Let  $F_1^S(\theta)$  and  $F_2^S(\theta)$  be the source field patterns from each antenna edge  $Q_{s1}$  and  $Q_{s2}$  in the presence of the strip scatterer, respectively. Similar to Equation (3-4), it is easy to see from Figure 15 that

$$F_i^S(\theta) = \begin{cases} 0 & \text{for } \theta_{i1}^S < \theta < \theta_{i2}^S \\ E_0 \cdot D_{Ii} e^{jky_{Si} \sin \theta} & \text{elsewhere,} \end{cases} \quad (5-9)$$

where  $D_{I1}$  and  $D_{I2}$  are defined in Equation (5-2). By superposition, the total source field pattern  $F^S(\theta)$  is given by

$$F^S(\theta) = F_1^S(\theta) + F_2^S(\theta). \quad (5-10)$$

As shown in Figure 16, in regions I and V, there are source fields from both  $Q_{s1}$  and  $Q_{s2}$ . In regions II and IV, there is only one source field from either  $Q_{s2}$  or  $Q_{s1}$ . There is no source field in region III. Note that there may be no region III in the far field if the scatterer is small compared to the source.

b. Reflection from the scatterer

Then, similar to Equation (3-6), the contribution of the reflected field from point  $Q_{Ii}$  is given by

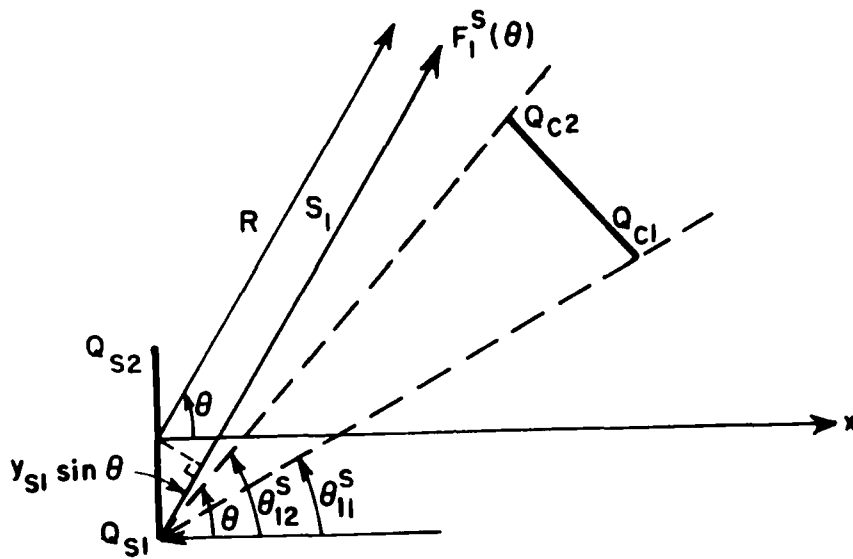


Figure 15. The source field of the two-point GTD with the scatterer present.

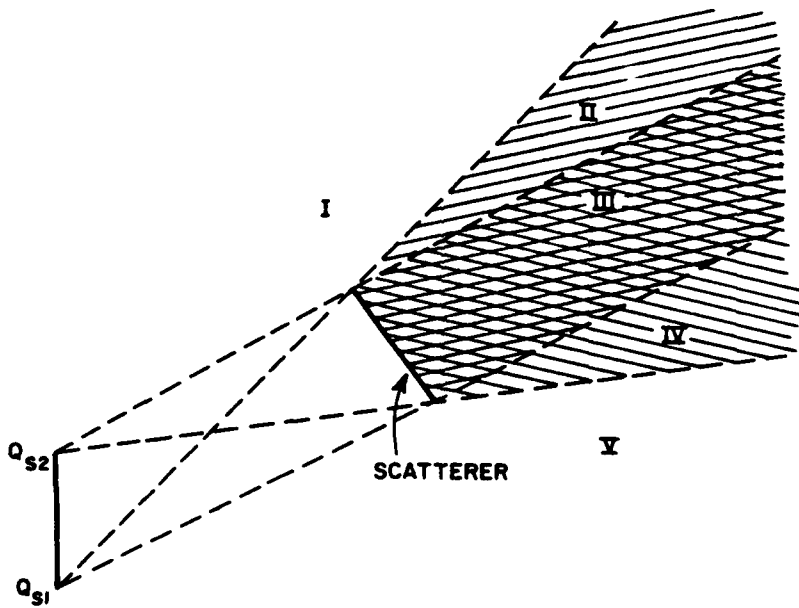


Figure 16. The shadow regions of the source fields.

$$F_i^R(\theta) = \begin{cases} \mp E_0 D_{Ii}(R; \pi - \theta_R) e^{j\psi_{Ri}} & \text{for } \theta_{i2}^R < \theta < \theta_{i1}^R, \text{ and} \\ 0 & \text{elsewhere,} \end{cases} \quad (5-11)$$

where  $i = 1$  or  $2$ ,

$R \rightarrow \infty$  for the far field,

$\theta_R = 2\Delta\theta - \theta - \pi$ ,

$\Delta\theta$  is the tilt angle of the strip scatterer

and  $\psi_{Ri} = k(x_{Ii} \cos\theta + y_{Ii} \sin\theta)$ .

Note that  $\theta_{i1}^R$  and  $\theta_{i2}^R$  are the shadow angles of edge  $Q_{Ii}$  as shown in Figure 17. The reflected field regions are shown in Figure 18. In regions II and IV, there are reflected fields from the edge only. In region III, there are reflected fields from both edges. There are no reflected fields in regions I and V. Again, there may be no region III in the far zone.

#### c. Diffraction from the scatterer

Since each source point on the antenna illuminates both edges of the scatterer, there are 4 diffracted terms. The field from source point  $Q_{Si}$  incident on the edge  $Q_{Cj}$  of the scatterer is given by

$$E_{ij}^I = E_0 D_{Si} \frac{e^{-jks_{ij}}}{\sqrt{s_{ij}}} \quad \text{for } i=1,2 \text{ and } j=1,2, \quad (5-12)$$

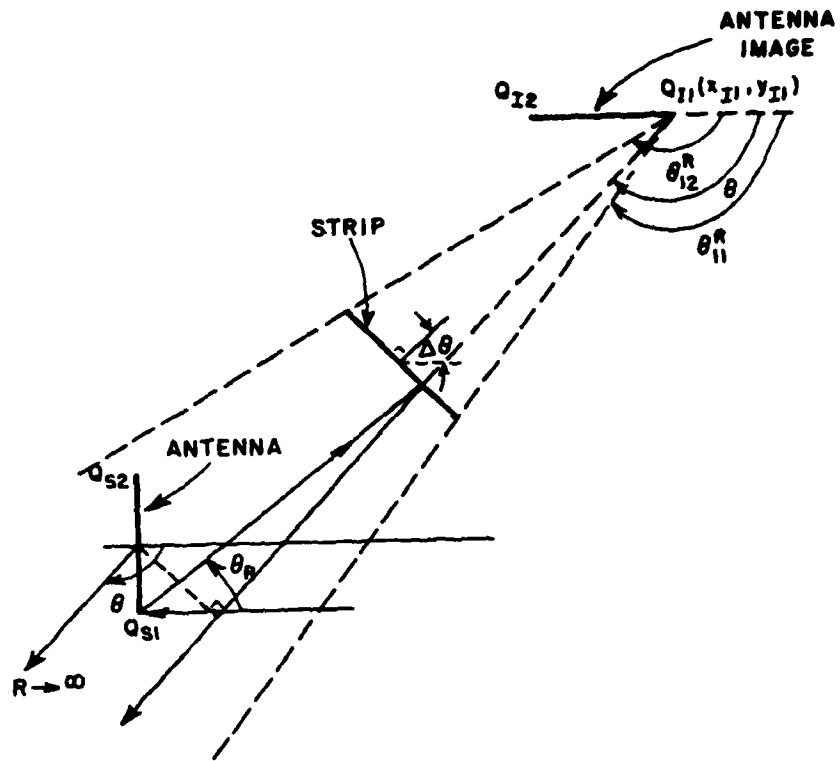


Figure 17. The reflected field of the two-point GTD method.

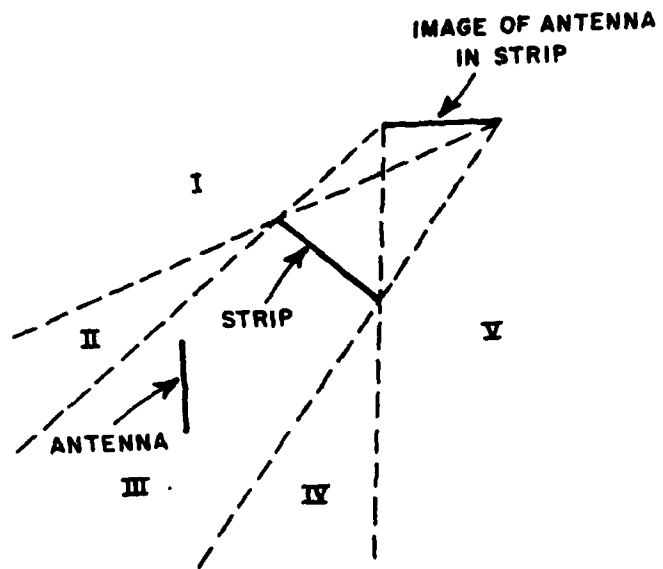


Figure 18. The illuminated regions of the reflected fields.

where  $D_{Ii}$  and  $S_{ij}$  have been defined in Equation (5-2) and Equation (5-7) respectively. The pattern function of the total diffracted field  $F^d(\theta)$  is the sum of the 4 terms such that

$$F^d(\theta) = \sum_{i=1}^2 \sum_{j=1}^2 F_{ij}^d(\theta), \quad (5-13)$$

where  $F_{ij}^d(\theta)$  corresponds to the diffracted field of source  $Q_{Si}$  from edge  $Q_{Cj}$ , which is given by

$$F_{ij}^d(\theta) = E_{ij}^I \cdot D_{ij} e^{j\psi_{dj}} \quad \text{for } i=1,2 \text{ and } j=1,2. \quad (5-14)$$

Similar to Equation (3-10), the diffraction coefficients are given by

$$D_{ij} = D_I(L_{ij}; \phi_{ij} - \phi'_{ij}) + D_I(L_{ij}; \phi_{ij} + \phi'_{ij}) \quad (5-15)$$

and

$$L_{ij} = \frac{s_{ij} \cdot s_j}{s_{ij} + s_j} \rightarrow s_{ij} \quad \text{as } s_j \rightarrow \infty. \quad (5-16)$$

Note that  $\phi'_{ij}$  and  $\phi_{ij}$  are the incident and diffracted angles from  $Q_{Si}$  to  $Q_{Cj}$ , respectively, as shown in Figure 19.

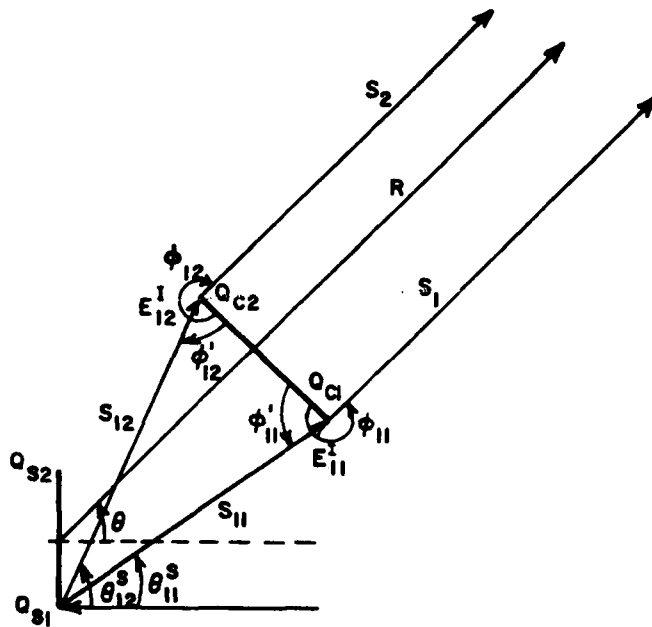


Figure 19. The diffracted fields of the two-point GTD method.

B. Source Distribution with Zero Edge Illumination

In the previous section, only the special case of a uniform current distribution across the antenna aperture plane was discussed. In order to solve the more general case, a source distribution with zero edge illumination is considered in this section. The combination of these two methods can be applied to most practical source distributions using superposition of the above two distributions.

1. Source field without the scatterer

For any source distribution with zero edge illumination but a non-zero slope at the edge, the source field may be calculated using

slope diffraction as long as it is reasonably far from the main beam. An incident plane wave  $E^i$  with a cosine distribution as shown in Figure 20 is used as an example in this section, where  $E^i = \cos(\frac{\pi y}{L})$  and the width of the aperture antenna is given by  $L$ . Then the slope diffraction from one antenna edge is given by Equation (2-26), such that

$$E_i^S = \frac{1}{jk} \frac{\partial E^i(Q_{S_i})}{\partial n} D_{pI}(s_i; \phi_i + \phi_i') \frac{e^{-jks_i}}{\sqrt{s_i}} \text{ for } i=1, \text{ or } 2, \quad (5-17)$$

where  $\frac{\partial E^i(Q_{S_1})}{\partial n} = \frac{\partial [\cos(\frac{y\pi}{L})]}{\partial (-y)} \Big|_{y=-\frac{L}{2}} = -\frac{\pi}{L},$

$$\frac{\partial E^i(Q_{S_2})}{\partial n} = \frac{\partial [\cos(\frac{y\pi}{L})]}{\partial y} \Big|_{y=\frac{L}{2}} = -\frac{\pi}{L}, \quad (5-18)$$

$$\phi_1' = \phi_2' = \frac{\pi}{2}, \quad \phi_1 = \frac{\pi}{2} - \theta, \quad \phi_2 = \frac{\pi}{2} + \theta, \text{ and}$$

$$D_{pI}(s_i; \phi_i + \phi_i') = \frac{\partial D_I(s_i; \phi_i + \phi_i')}{\partial \phi_i'} \quad (5-19)$$

Note that  $s_1 = R - y_{S_1} \sin \theta$ , and  $s_2 = R - y_{S_2} \sin \theta$ . The total source field  $E^S$  is given by

$$E^S = E_1^S + E_2^S$$

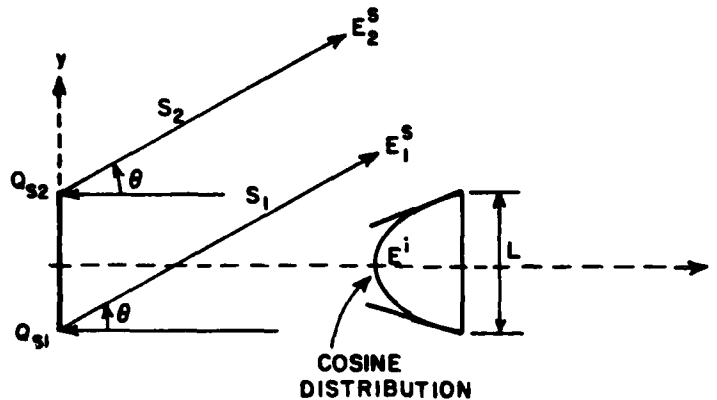


Figure 20. A cosine source distribution modeled by two-point GTD.

So the far field pattern function  $F^S(\theta)$  is obtained from Equation (5-17) as

$$F^S(\theta) = \frac{s_0}{jk} \left[ D_{pI}(s_1; \pi - \theta) e^{jky_{s1} \sin \theta} + D_{pI}(s_2; \pi + \theta) e^{jky_{s2} \sin \theta} \right] \quad (5-20)$$

where  $s_0 \triangleq \frac{\Delta}{\partial n} \frac{\partial E^i}{\partial n}$ , which is equal to  $-\frac{\pi}{L}$  for the cosine distribution.

## 2. Total solution with the strip scatterer present

The source, reflected, and diffracted fields are evaluated in the same way as in the previous procedure except that the source fields correspond to those of the slope diffractions from the antenna edges. The equations for the various field contributions are given in the following sections.

a. Source field with the scatterer

Let  $F_i^S(\theta)$  represent the source field pattern from the antenna edge at  $\theta_{s_i}$ , where  $i=1$  or  $2$ , as shown in Figure 15. Thus

$$F_i^S(\theta) = \begin{cases} 0 & \text{for } \theta_{i1}^S < \theta < \theta_{i2}^S, \text{ and} \\ \frac{s_0}{jk} D_{pI}(s_i; \phi_i + \phi_i^!) e^{jky_{s_i} \sin \theta} & \text{elsewhere,} \end{cases} \quad (5-21)$$

where  $s_0 = \frac{\partial E^i}{\partial n}$  and  $D_{pI}$  is defined in Equation (2-26), and all other parameters are the same as in Equation (5-9). Then, the total source field with the scatterer present is given by

$$F^S(\theta) = \sum_{i=1}^2 F_i^S(\theta). \quad (5-22)$$

b. The reflected field

Referring to Figure 17, the pattern of the reflected field from the  $i$ th edge of the source is given by

$$F_i^R(\theta) = \begin{cases} \mp \frac{s_0}{jk} D_{pI}(R; \pi - \theta_R) e^{j\psi_{Ri}} & \text{for } \theta_{i2}^R < \theta < \theta_{i1}^R, \text{ and} \\ 0 & \text{elsewhere,} \end{cases} \quad (5-23)$$

where  $\psi_{Ri}$ ,  $R$ , and  $\theta_R$  are the same as those in Equation (5-11). The total reflected field  $F^R(\theta)$  is the sum of  $F_1^R(\theta)$  and  $F_2^R(\theta)$  as done previously.

c. The diffracted field

As shown in Figure 19, the incident field  $E_{ij}^I$  is given by Equation (5-17), such that

$$E_{ij}^I = \frac{s_0}{jk} D_{pI}(s_i; \phi_i + \phi_i') \frac{e^{-jks_{ij}}}{\sqrt{s_{ij}}} \quad (5-24)$$

Then, following the previous procedure, one finds

$$F_{ij}^{sd}(\theta) = E_{ij}^I \cdot D_{ij} \cdot e^{j\psi_{dj}}, \quad (5-25)$$

where  $D_{ij}$  and  $\phi_{dj}$  have been previously defined by Equations (5-15) and (3-12). Then the total diffracted field pattern is given by

$$F^{sd}(\theta) = \sum_{i=1}^2 \sum_{j=1}^2 F_{ij}^{sd}(\theta). \quad (5-26)$$

CHAPTER VI  
SLOPE DIFFRACTION FROM THE SCATTERER

As mentioned in Chapter I, when the strip scatterer is located near the projected aperture of the antenna, slope diffraction from the edges of the scatterer must also be included. Large aperture antennas generally have rapid field variations which implies that the field incident on the edge of scatterer may likely have a very significant slope. This is illustrated in Figure 34 in the next chapter. It was found that slope diffraction models the rapid source field variations very well for a uniform source distribution if the scatterer is not too close to the projected aperture. However, slope diffraction does not work so well for a cosine source distribution (see Figure 38) because the source field varies too rapidly.

The geometry used to evaluate the slope of the incident field is shown in Figure 21, where the latter is numerically approximated by

$$\frac{\partial E_{ij}^I}{\partial n} = \frac{E_{ij}^{I'} - E_{ij}^I}{\Delta n} \quad , \quad (6-1)$$

with  $E_{ij}^{I'}$ ,  $E_{ij}^I$ ,  $\Delta n$ ,  $\theta_{ij}^{S'}$ , and  $s_{ij}'$  defined in Figure 21. So the contributions from the slope diffraction terms are given by

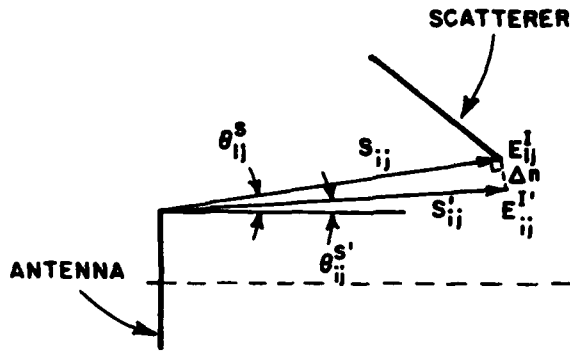


Figure 21. The geometry used to calculate the slope of the incident field.

$$F_{\text{slope}}^d(\theta) = \sum_{i=1}^2 \sum_{j=1}^2 \frac{1}{jk} \frac{\partial E_{ij}^i}{\partial n} P_{ij} e^{jk\psi_{dj}}, \quad (6-2)$$

where the slope diffraction coefficient  $P_{ij} \triangleq \partial D_{ij} / \partial \phi'$  is given by

$$P_{ij} = D_{pI}(s_{ij}, \phi_{ij} - \phi'_{ij}) \pm D_{pI}(s_{ij}, \phi_{ij} + \phi'_{ij}), \quad (6-3)$$

where  $s_{ij}$ ,  $\phi_{ij}$ , and  $\phi'_{ij}$  are shown in Figure 19, and  $D_{pI}$  is defined by Equation (2-26). Recall that the "+" sign is used for the TE case and the "-" sign for the TM case.

CHAPTER VII  
RESULTS AND DISCUSSIONS

In the previous chapters, two approaches are developed for calculating the effect of a strip scatterer on the antenna pattern: a) the large subaperture technique and b) the two-point GTD source field method. Both approaches use the GTD method to calculate the scattering from structures in a manner similar to that used in the present codes [1,2]. In this chapter, results are given to show the effects and limitations of the two approaches. The results of the large subaperture technique for the source field are compared in Section A with those from the original GTD method which uses superposition from small elements. The accuracy and efficiency of the two-point GTD source field method are shown in Section B. Next, when the strip scatterer is located near the projected aperture, slope diffraction can be used to improve the results for the GTD source field methods as discussed in Chapter VI. The effect of slope diffraction from the scatterer and its limitations are shown in Section C. Finally, the effect of the various scatterer geometries and locations are shown in Section D. A  $10\lambda$  source antenna is used in these results and two types of source distributions are included: type

1 is for the cases of uniform source distribution and type 2 is for the cosine source distribution.

#### A. Large Subaperture Technique

As mentioned in Chapter I, the large subaperture technique works well as long as the size of the subaperture is no larger than 1 to 2 wavelengths.

##### 1. Type 1 - Uniform source distribution

The source field of the uniform distribution (type 1) without the scatterer present is shown in Figure 22. Note that it exists in the region of  $-90^{\circ} \leq \theta \leq 90^{\circ}$  only. The far field patterns are shown in Figures 23 and 24 for two different scatterer geometries. Both cases include  $1\lambda$  and  $2\lambda$  subaperture sizes and are compared to the results using small  $\lambda/3$  elements. Note that there is almost no difference between the results using  $\lambda$  subapertures and  $\lambda/3$  elements as shown in Figures 23a and 24a. This method works very well for most regions even with  $2\lambda$  subapertures and used only 1/6 of the original CPU time as shown in Figures 23b and 24b.

##### 2. Type 2 - Cosine distribution

A cosine distribution is used to represent a source distribution with zero edge illumination in these examples. The results for type 2 are shown in Figures 25, 26 and 27 for the same antenna/scatterer geometries as were shown for type 1. The large subaperture technique does not work so well as it does for type 1 because the source field

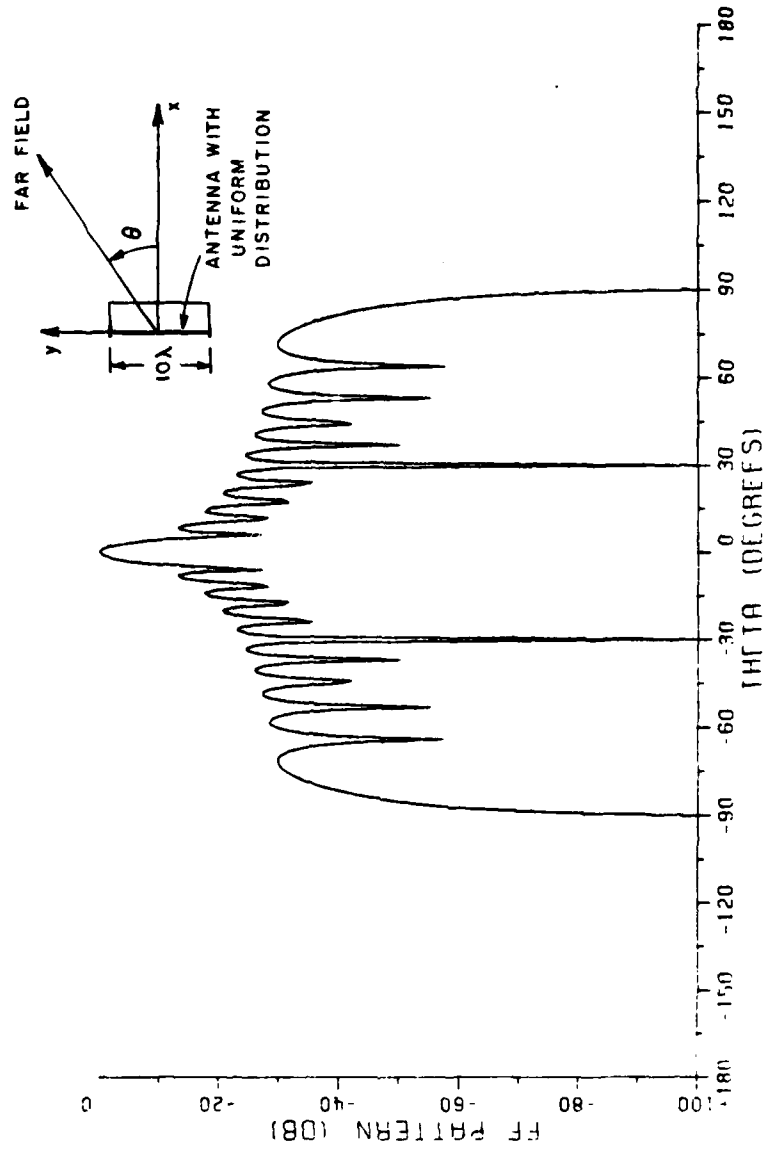


Figure 22. The far field pattern of a  $10\lambda$  antenna with uniform source distribution (type I antenna).

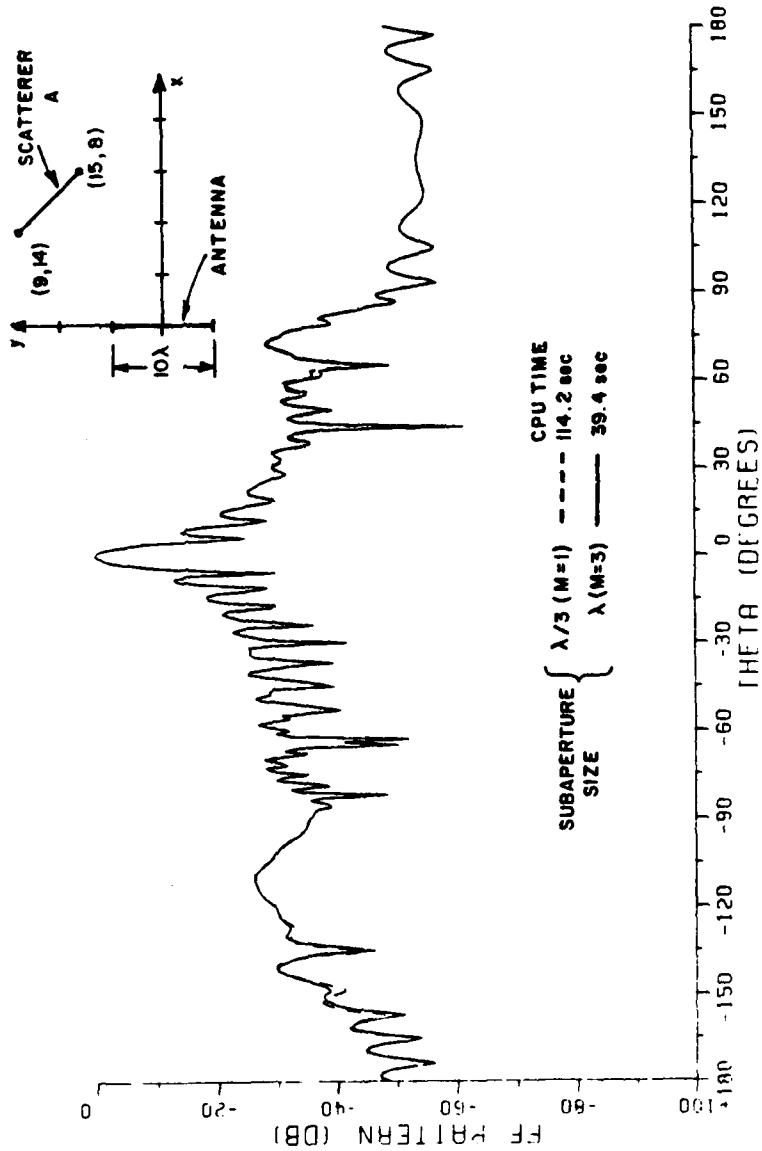


Figure 23a. The far field pattern of a  $10\lambda$  type 1 antenna with strip scatterer A. Large subaperture method compared to the original method using  $\lambda/3$  as an element.

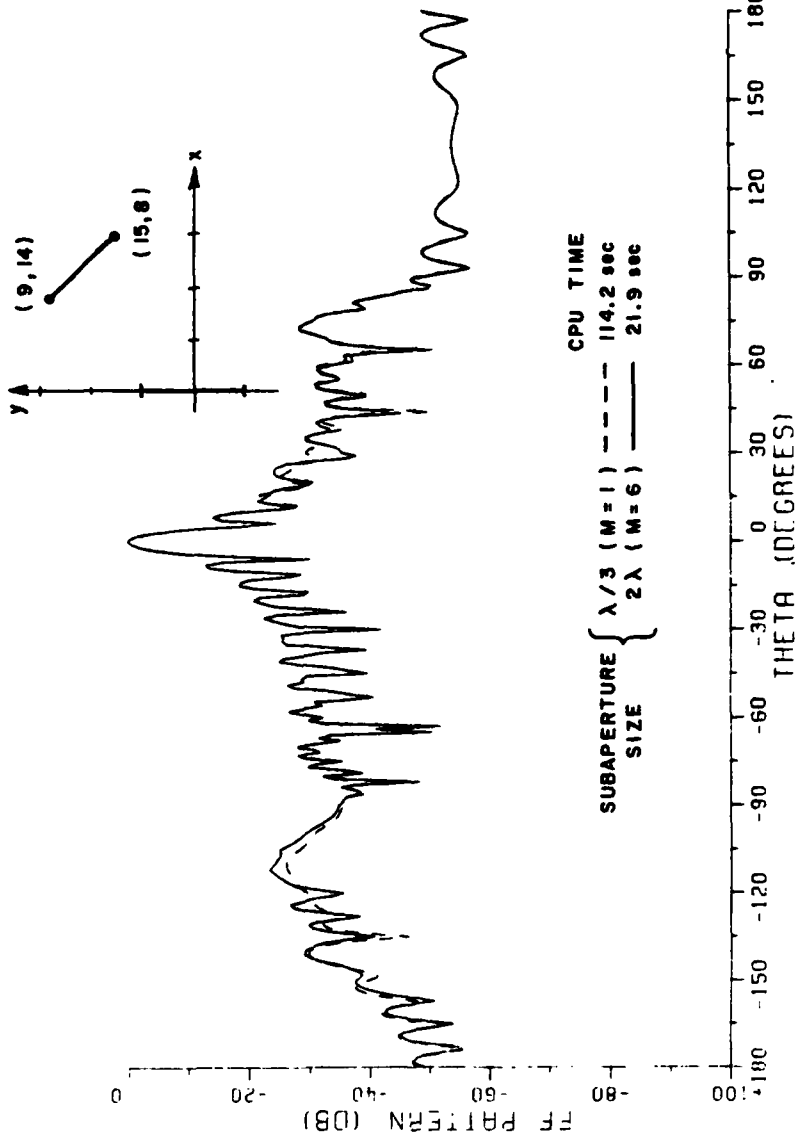


Figure 23b.

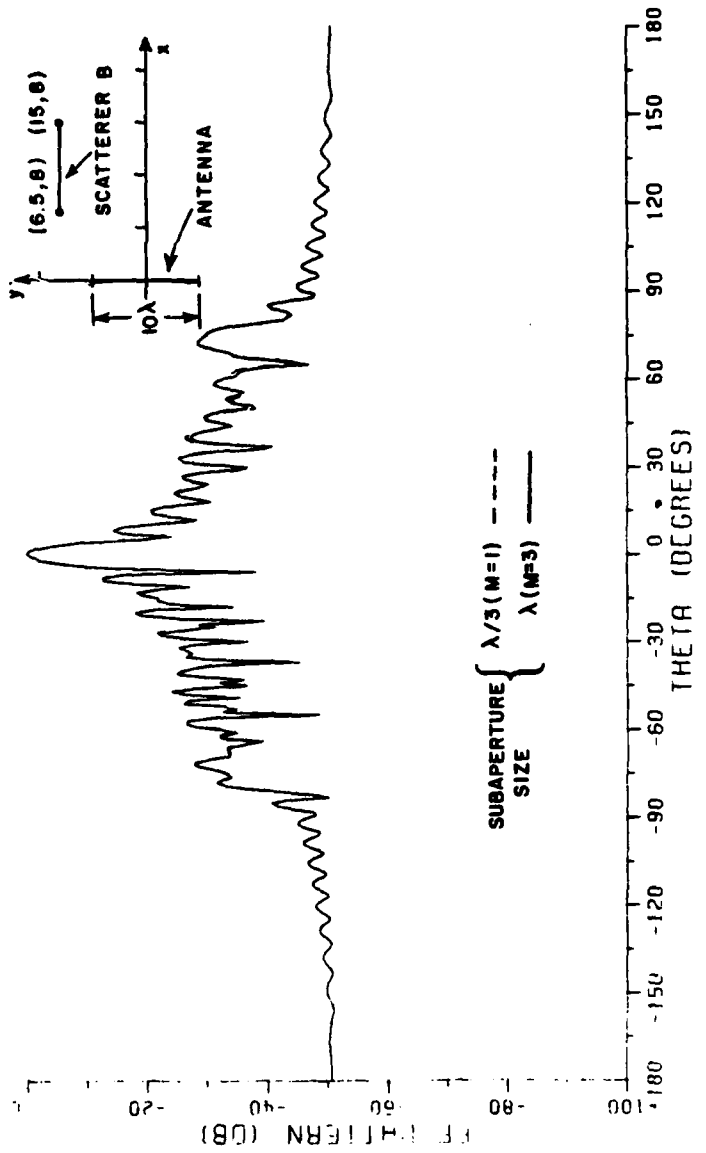


Figure 24a. The far field pattern of a  $10\lambda$  type 1 antenna with strip scatterer B.

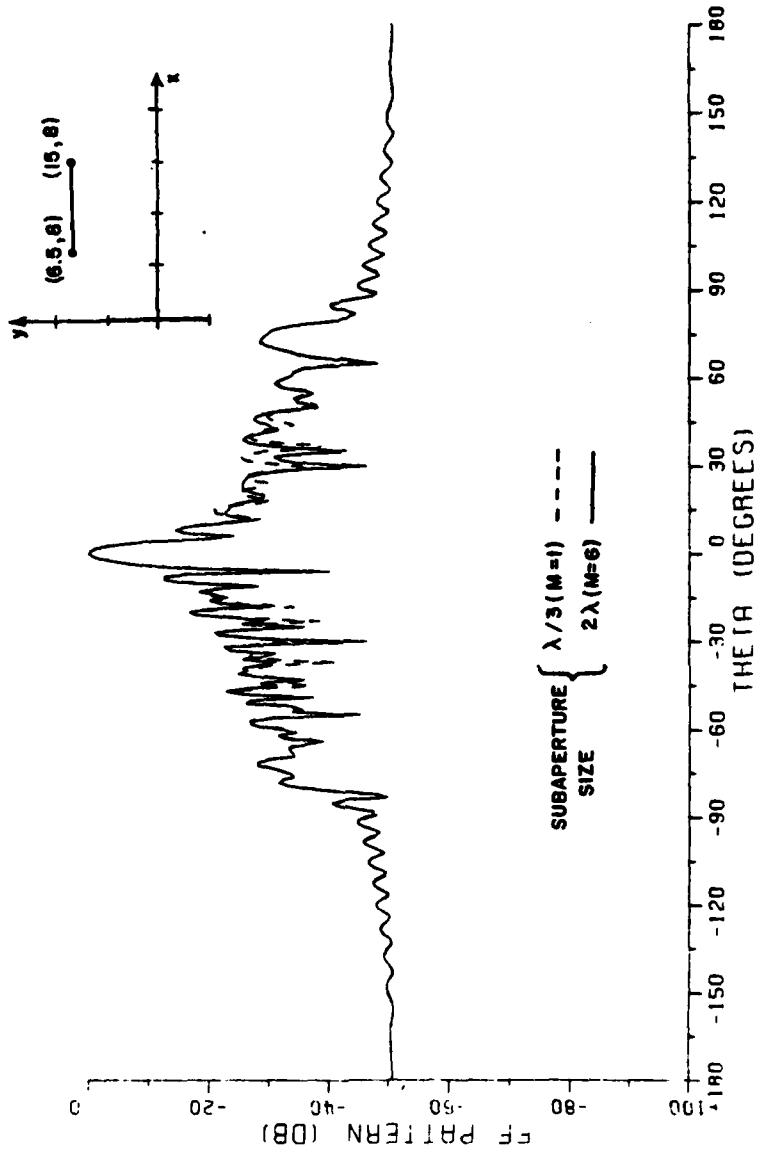


Figure 24b.

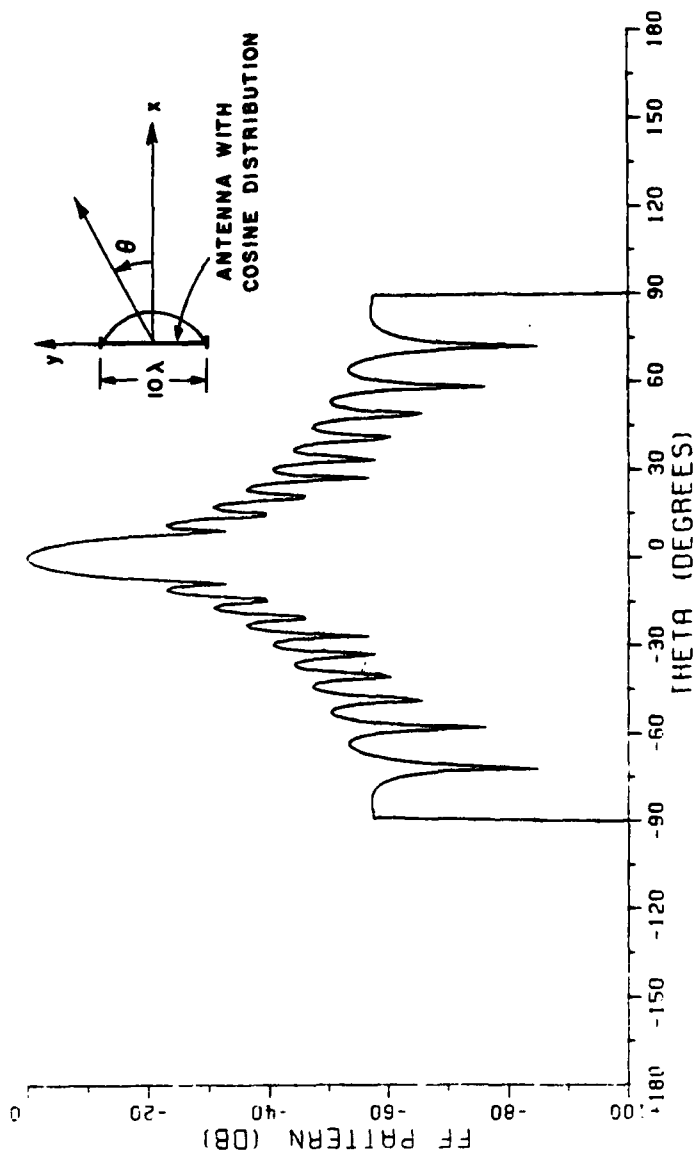


Figure 25. The far field pattern of a  $10\lambda$  antenna with cosine source distribution (type 2 antenna).

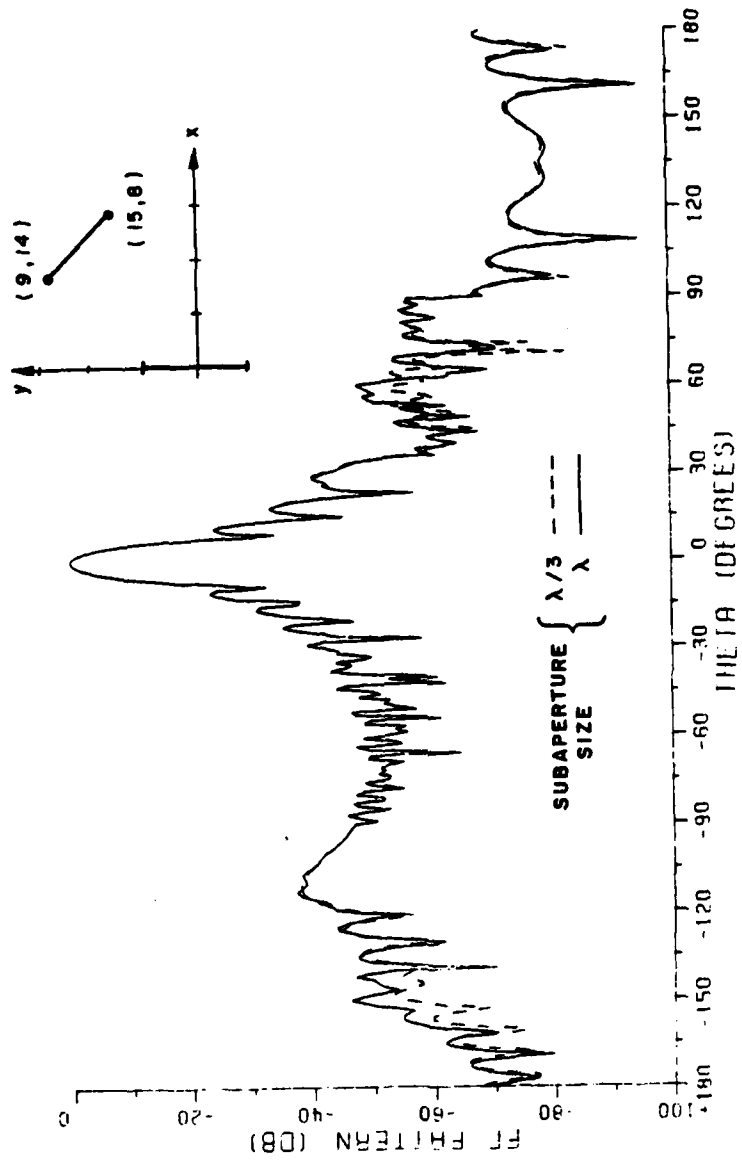


Figure 26a. The far field pattern of a  $10\lambda$  type 2 antenna with strip scatterer A.

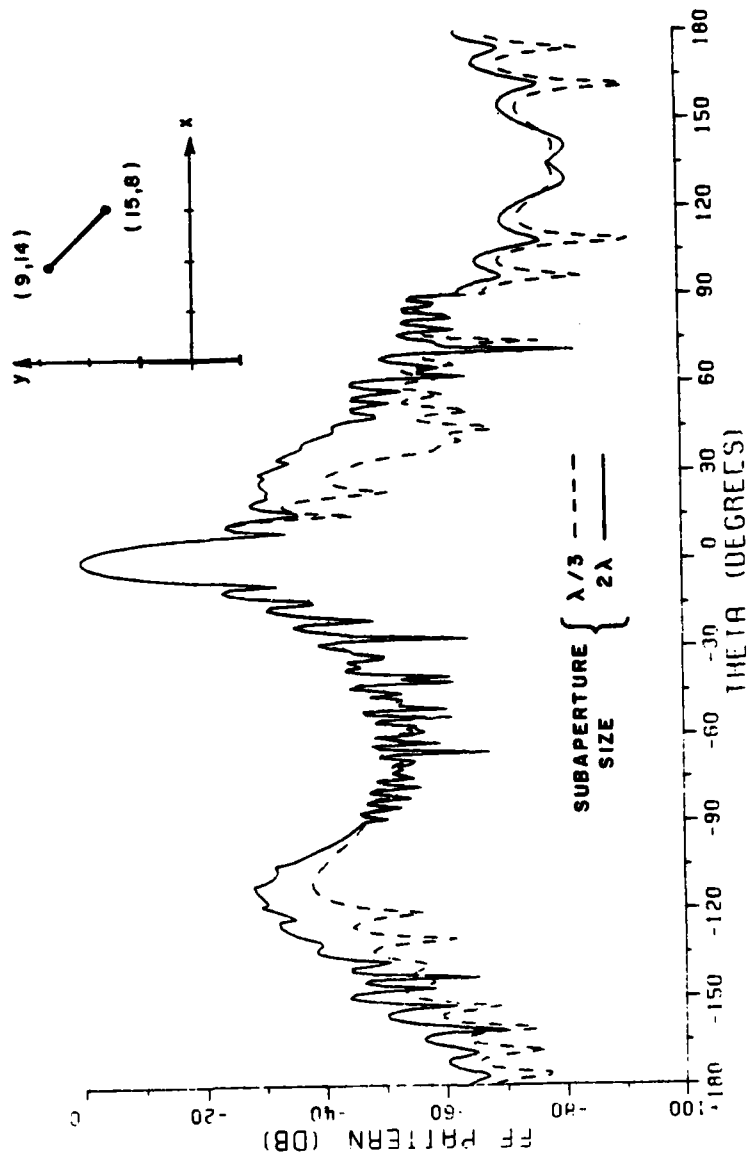


Figure 26b.

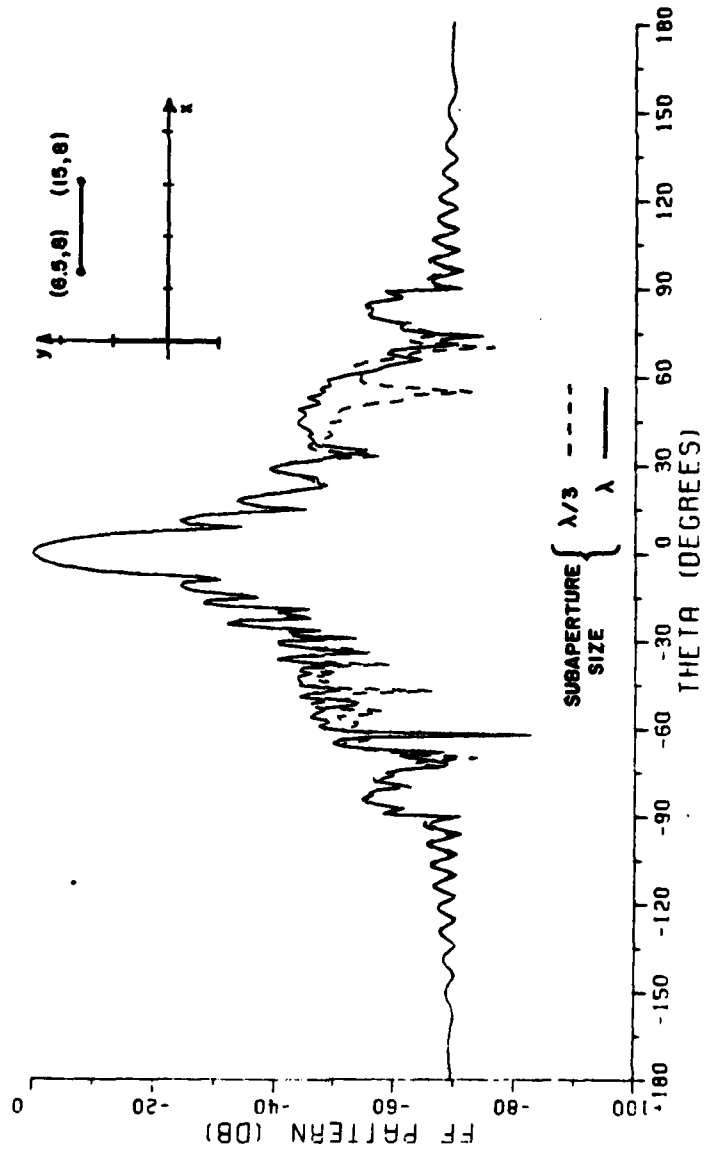


Figure 27a. The far field pattern of a  $10\lambda$  type 2 antenna with strip scatterer B.

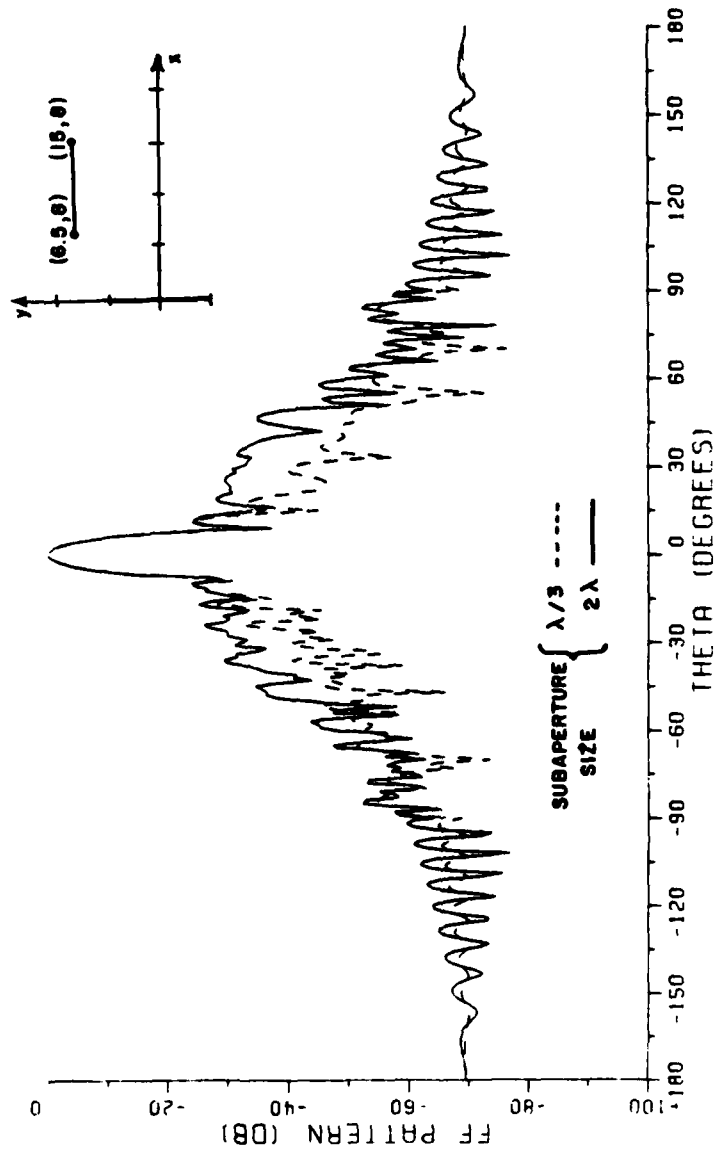


Figure 27b.

varies more sharply. For the result shown in Figure 26, the pattern value at angle  $-151^{\circ}$  was analyzed. Table I compares the individual contributions from each  $2\lambda$  section of the aperture (by using  $\lambda/3$  subapertures which is equivalent to the original method) to the contributions when the large subaperture method is used with  $2\lambda$  subapertures. Although the agreement between the contributions from each section is good, there is a large difference in the total fields. Note that the total field is small compared to the individual contribution as seen from Table I. This cancellation effect requires a very high accuracy for the individual contribution in order that the total field be accurately calculated.

#### B. Two-point GTD Source Field Method

The source field patterns without the scatterer present, as obtained by using two-point GTD, are shown in Figures 28 and 31 for source types 1 and 2, respectively. Note that: (1) GTD breaks down near the main beam and (2) the source fields in the back (i.e., for  $|\theta| > 90^{\circ}$ ) are omitted for the 2-point GTD in order to compare with the aperture integration source.

Figures 29, 30, 32, and 33 show the results of using the two-point GTD method. These results are compared to the results of using aperture integration (AI) for the source fields. It is apparent that 2-point GTD for the source field works very well in almost all regions except the main beam, where the GTD breaks down. The efficiency of the 2-point GTD method can be obtained by comparing the computer CPU time as follows. By using the AI source with  $\lambda/3$  elements for a  $10\lambda$

Table I

Contributions from each  $2\lambda$  section for the pattern values at  $\theta=151^\circ$  in Figure 26.

aperture section #	contribution by using $\lambda/3$ subapertures	contribution by using $2\lambda$ subapertures
1	$(-0.0205 + j0.0300) = 0.0364 / 124.3^\circ$	$(-0.0242 + j0.0315) = 0.0397 / 127.5^\circ$
2	$(0.0676 + j0.0009) = 0.0676 / 0.8^\circ$	$(0.0617 + j0.0145) = 0.0644 / 13.2^\circ$
3	$(-0.0471 - j0.0590) = 0.0756 / -128.6^\circ$	$(-0.0370 - j0.0562) = 0.0673 / -123.4^\circ$
4	$(-0.0031 + j0.0391) = 0.0392 / 94.5^\circ$	$(-0.0023 + j0.0352) = 0.0353 / 93.8^\circ$
5	$(0.0009 - j0.0061) = 0.0062 / -81.2^\circ$	$(-0.0006 - j0.0048) = 0.0048 / -97.0^\circ$
total field	$(-0.0022 - j0.0049) = 0.0054 / -114.5^\circ$	$(0.0024 + j0.0263) = 0.0265 / 95.2^\circ$

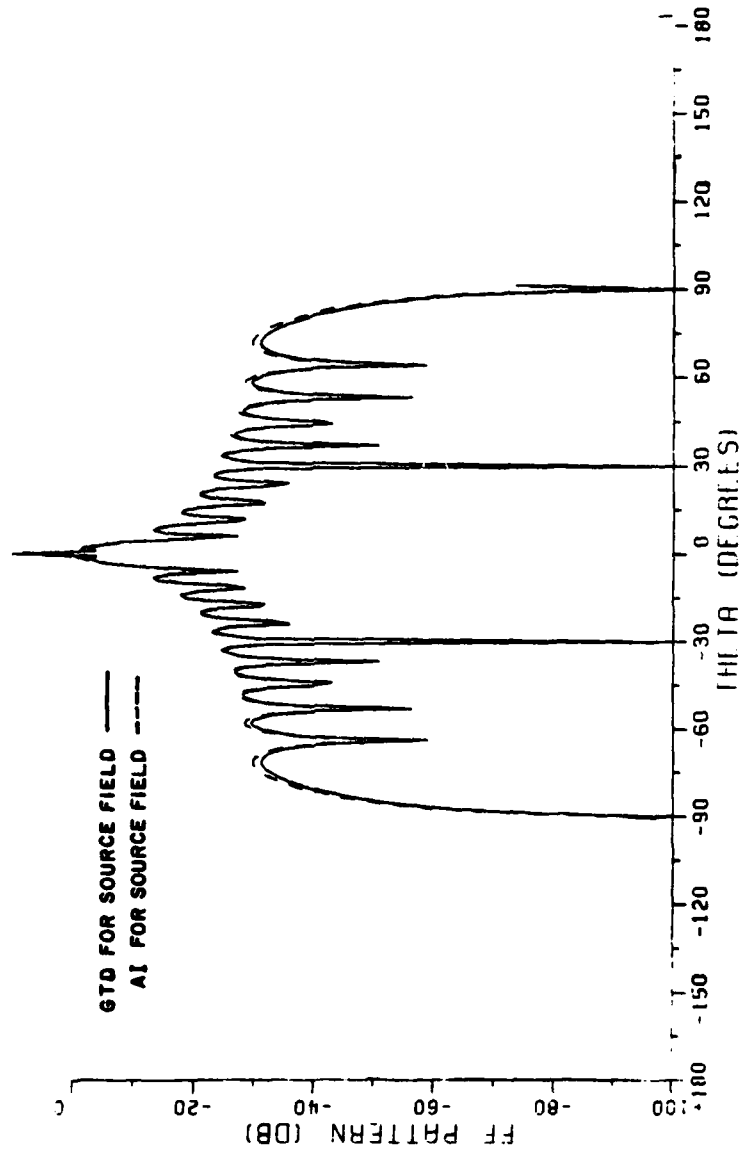


Figure 28. The far field pattern of a  $10\lambda$  type 1 antenna calculated by two-point GTD method with the field omitted in the region  $|\theta| \geq 90^\circ$ .

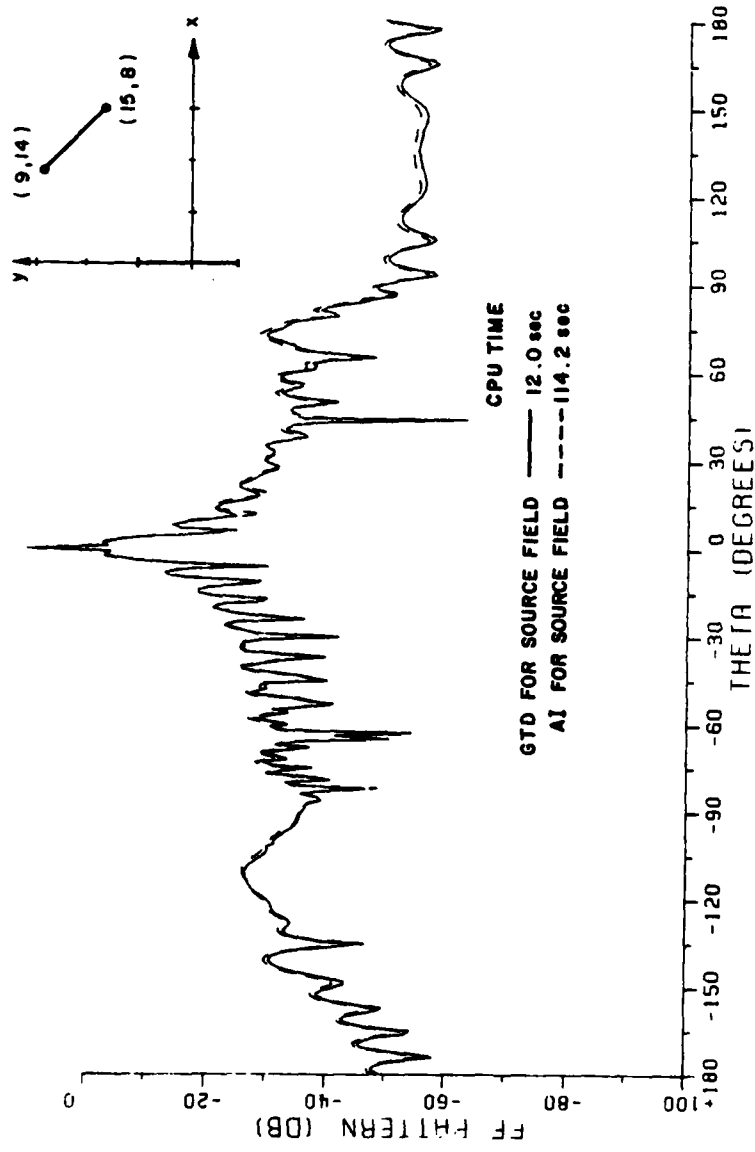


Figure 29. The far field pattern of a  $10\lambda$  type 1 antenna with scatterer A. Two-point GTD method compared to the original method using  $\lambda/3$  as an element.

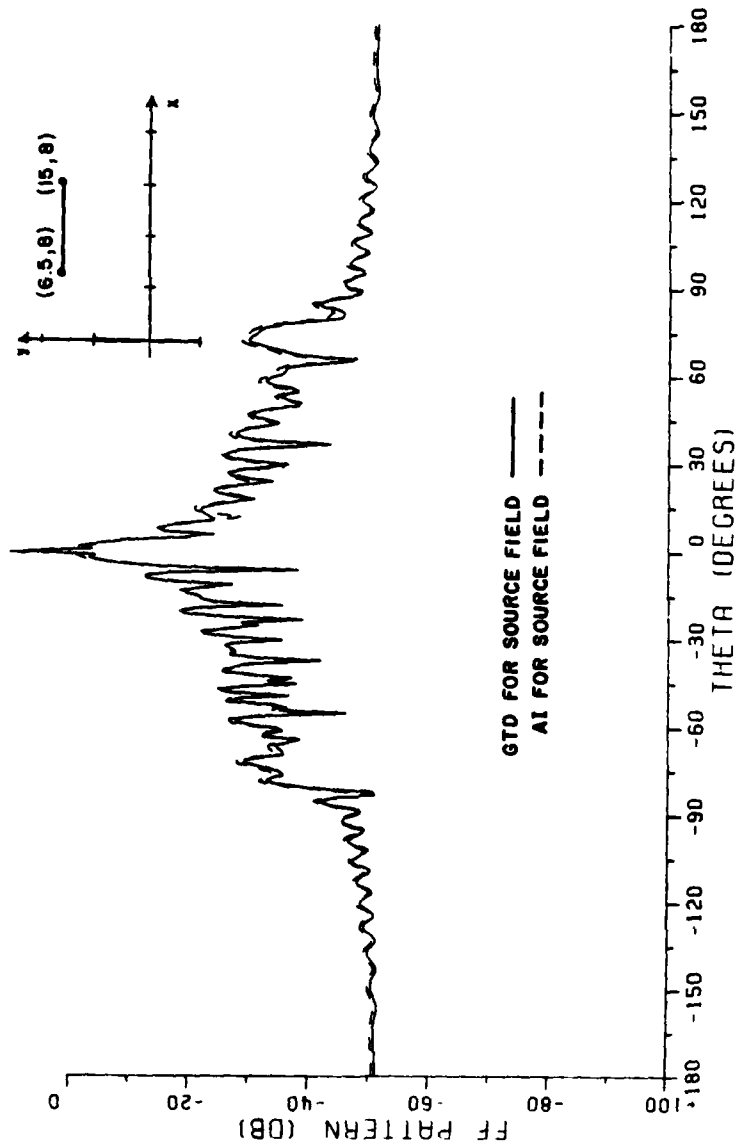


Figure 30. The far field pattern of a 10A type 1 antenna with scatterer B.

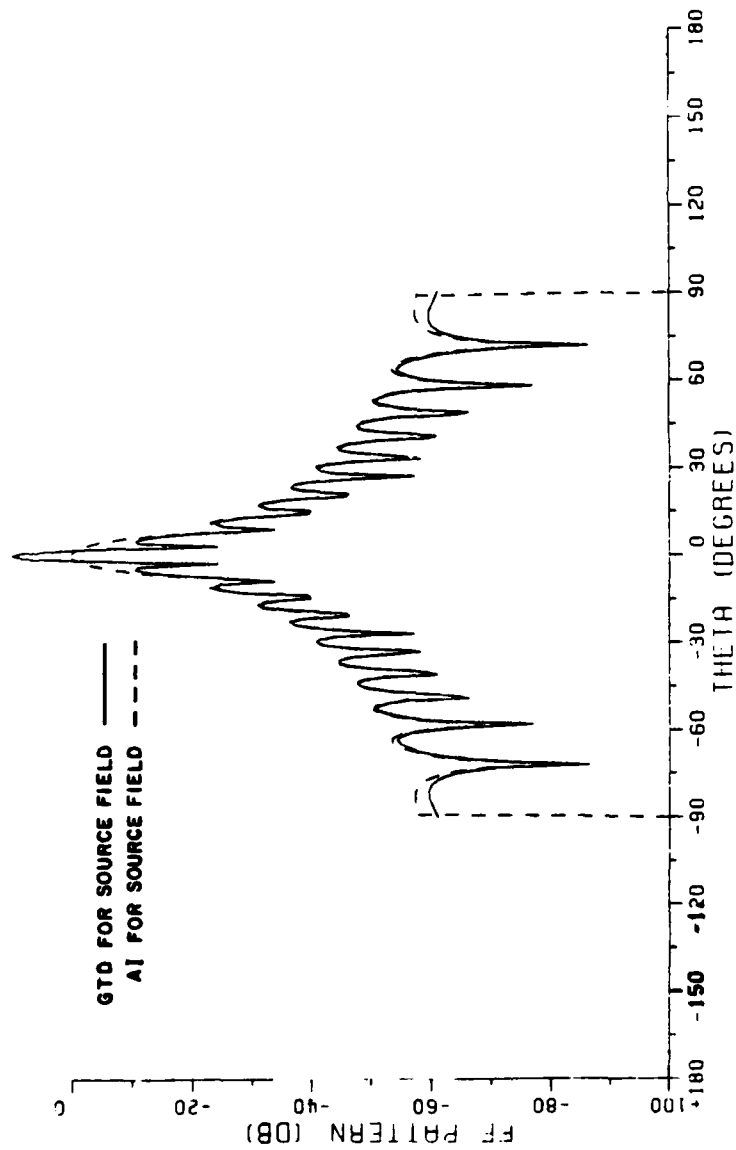


Figure 31. The far field pattern of a  $10\lambda$  type 2 antenna calculated by two-point GTD method with the field omitted in the range  $|\theta| > 90^\circ$ .

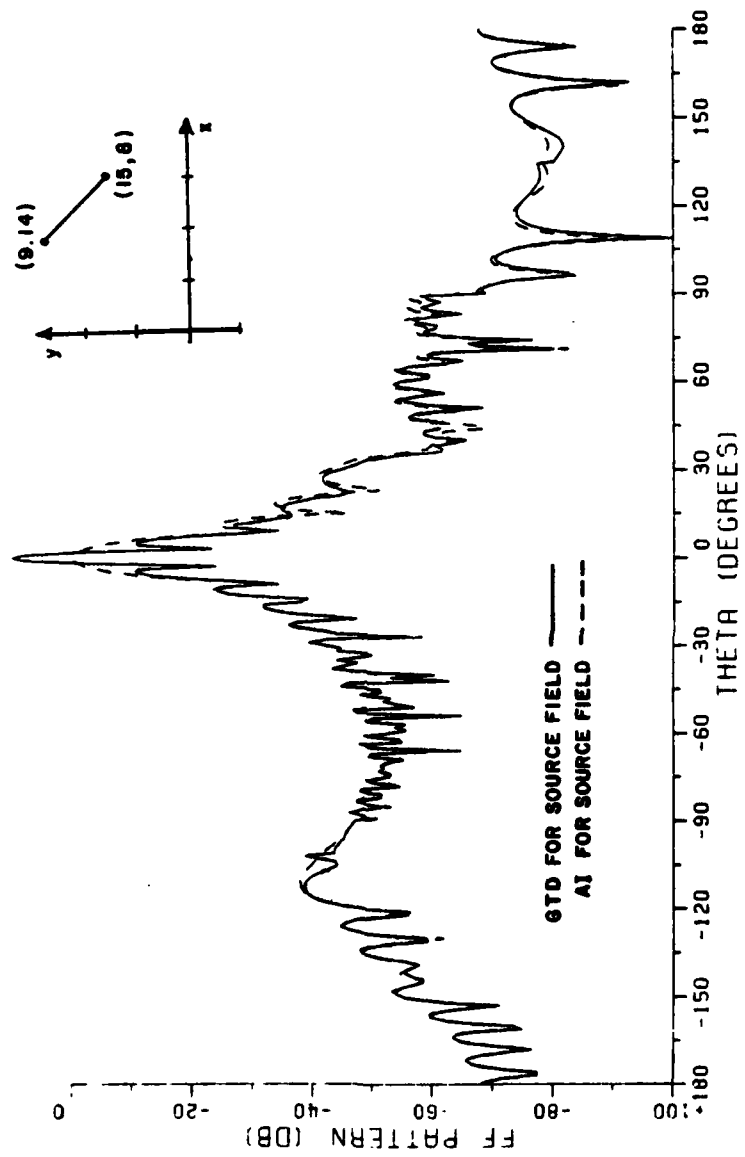


Figure 32. The far field pattern of a  $10\lambda$  type 2 antenna with scatterer A.

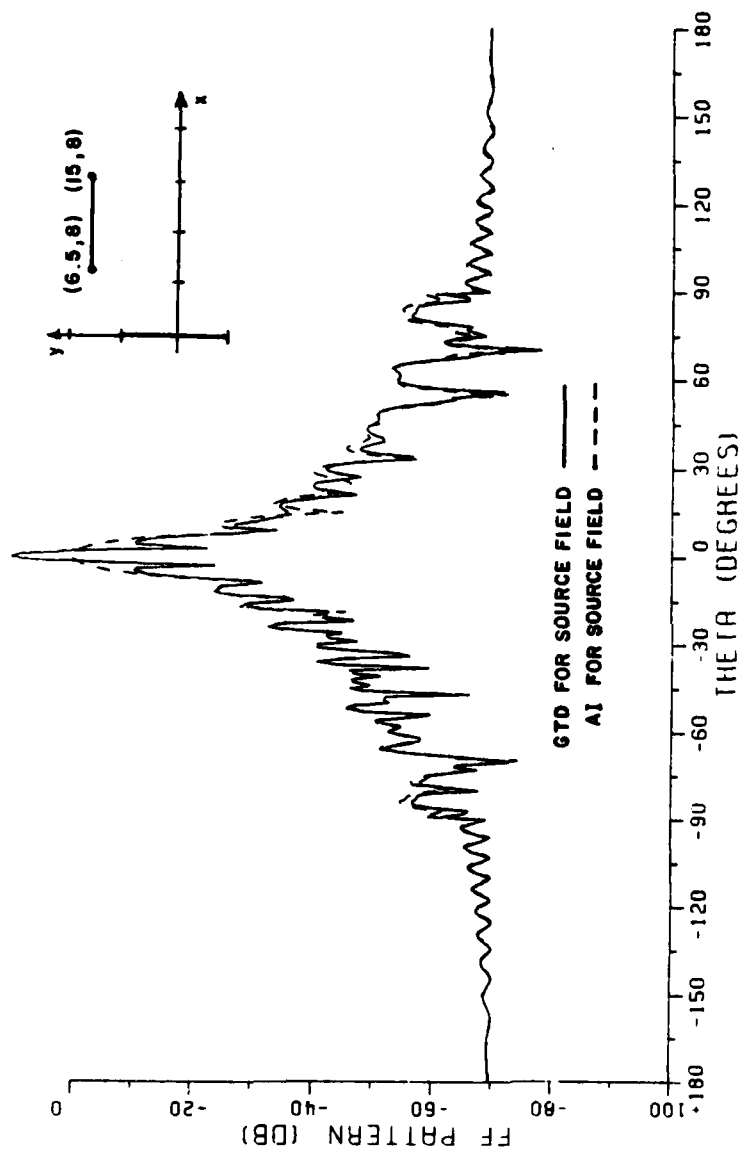


Figure 33. The far field pattern of a 10A type 2 antenna with scatterer B.

antenna (30 elements), it takes about 110 seconds to get the result shown in Figure 29. Since the CPU time is about proportional to the number of elements in the antenna, it will take more time if the antenna becomes larger. But by using two-point GTD method, no matter how large the antenna is, it only takes about 12 seconds.

C. Slope Diffraction from the Scatterer

As discussed in Chapter VI, slope diffraction from the scatterer is significant in some regions when the GTD source method is used and the scatterer is near the projected aperture of antenna. For type 1, if one edge of the scatterer is located  $3\lambda$  above the projected aperture of the antenna, slope diffraction can almost perfectly eliminate the slope discontinuity at the shadow boundary near  $\theta = -110^\circ$  for the reflected field as shown in Figure 34. But when the scatterer is located only  $1\lambda$  or  $2\lambda$  above the projected aperture, slope diffraction is not sufficient to solve the problem, as shown in Figures 35 and 36. The reason is that the source field is varying too sharply near the shadow boundary and can not be represented by a uniform plus slope field. For a cosine distribution, the incident field on the edges of the scatterer varies even more sharply and consequently, the problem becomes even more serious. As shown in Figures 37 and 38, slope diffraction is not enough to solve the problem in the small region near the reflected shadow boundaries until the scatterer is located about  $6\lambda$  above the projected aperture for this case.

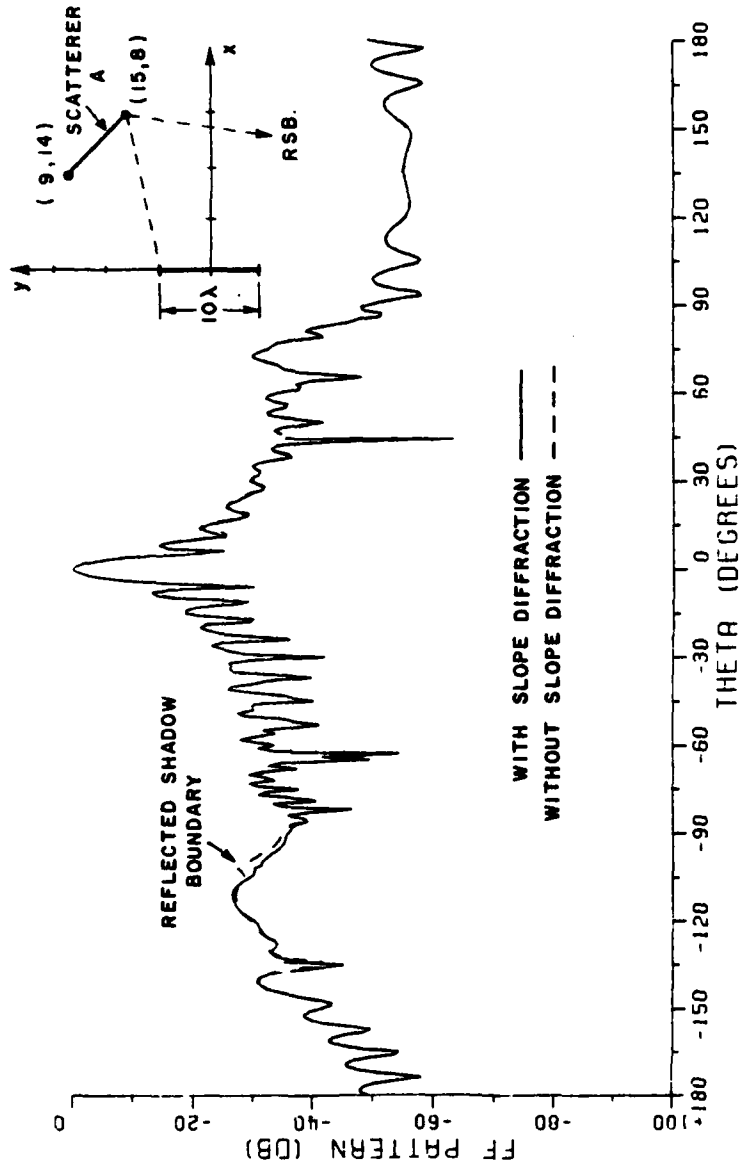


Figure 34. The effect of slope diffraction from the scatterer A for type 1 antenna.

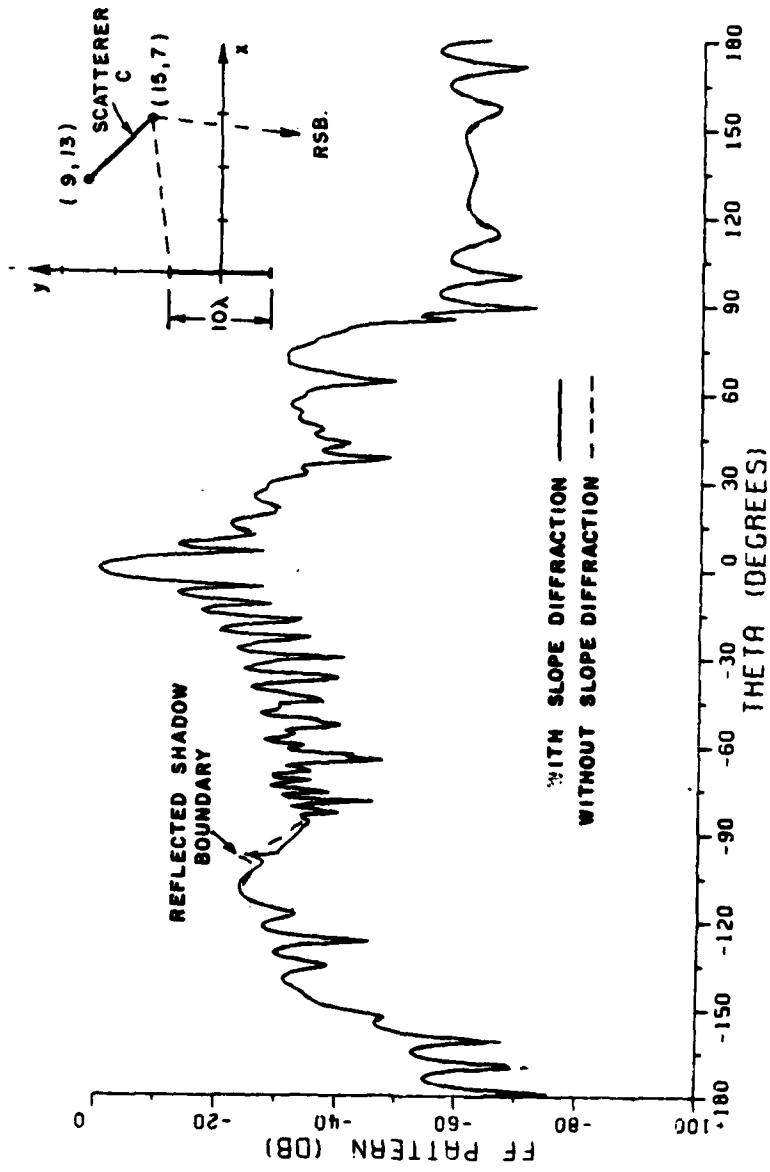


Figure 35. The effect of slope diffraction from the scatterer C for type 1 antenna.

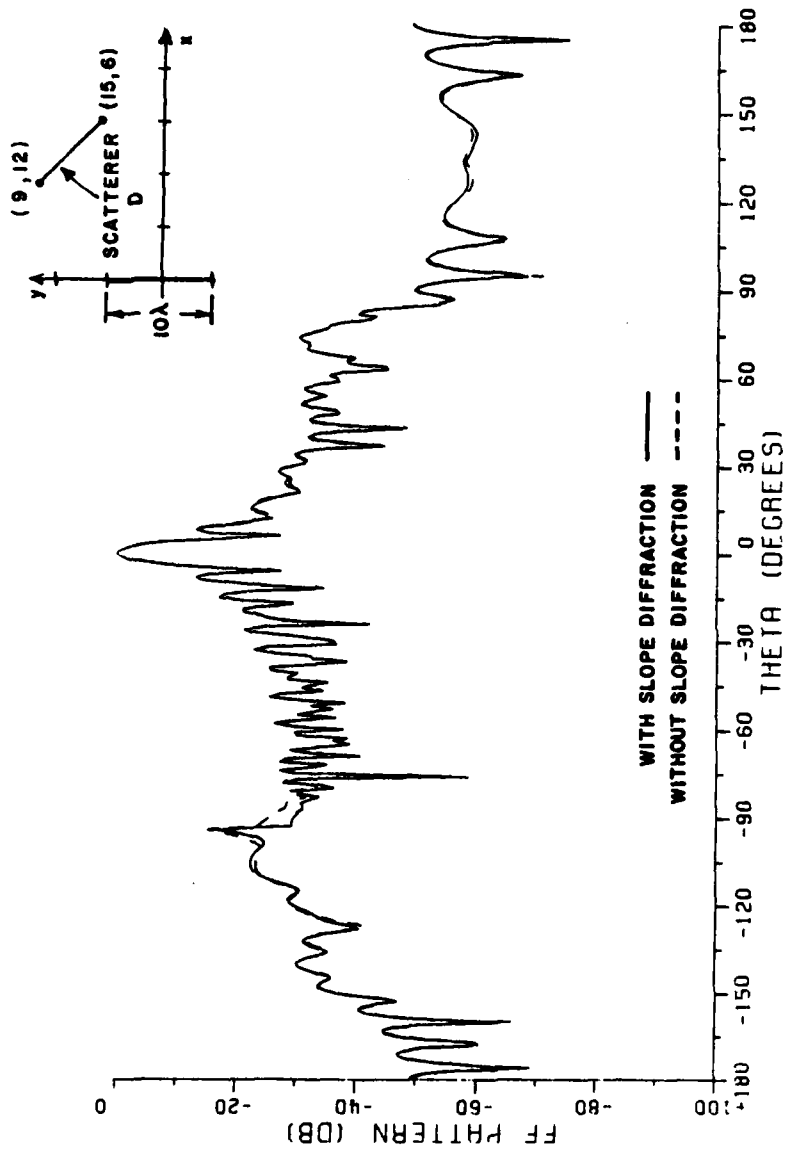


Figure 36. The effect of slope diffraction from the scatterer D for type 1 antenna.

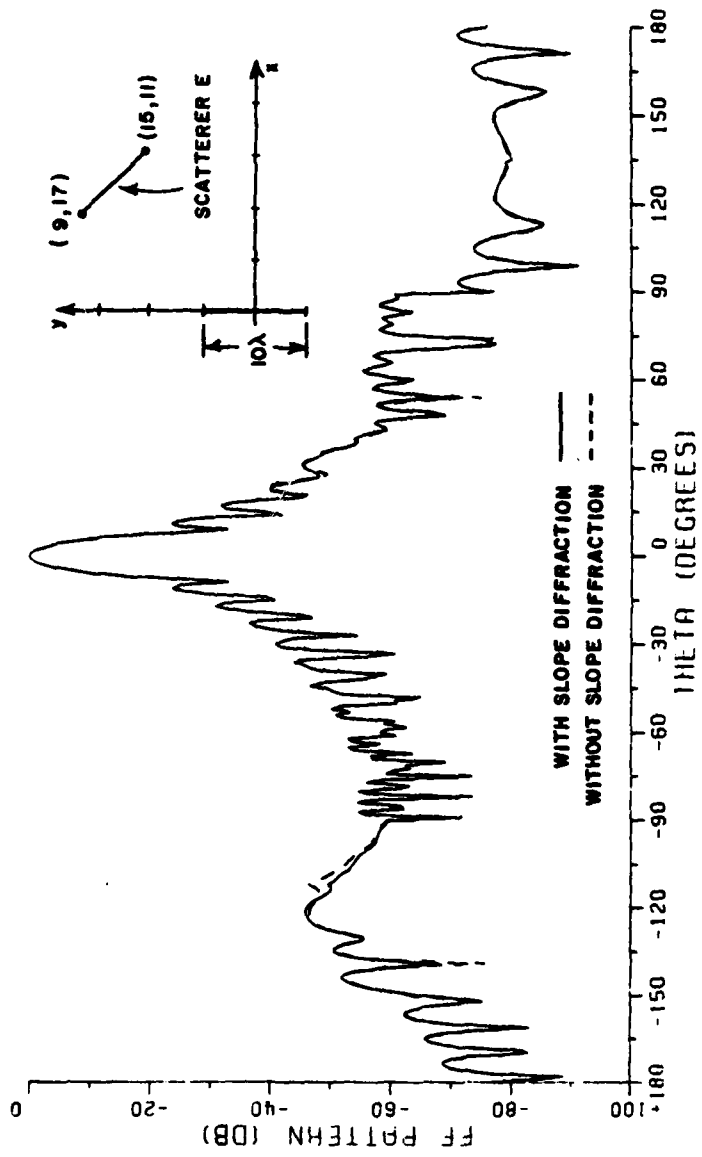


Figure 37. The effect of slope diffraction from the scatterer E for type 2 antenna.

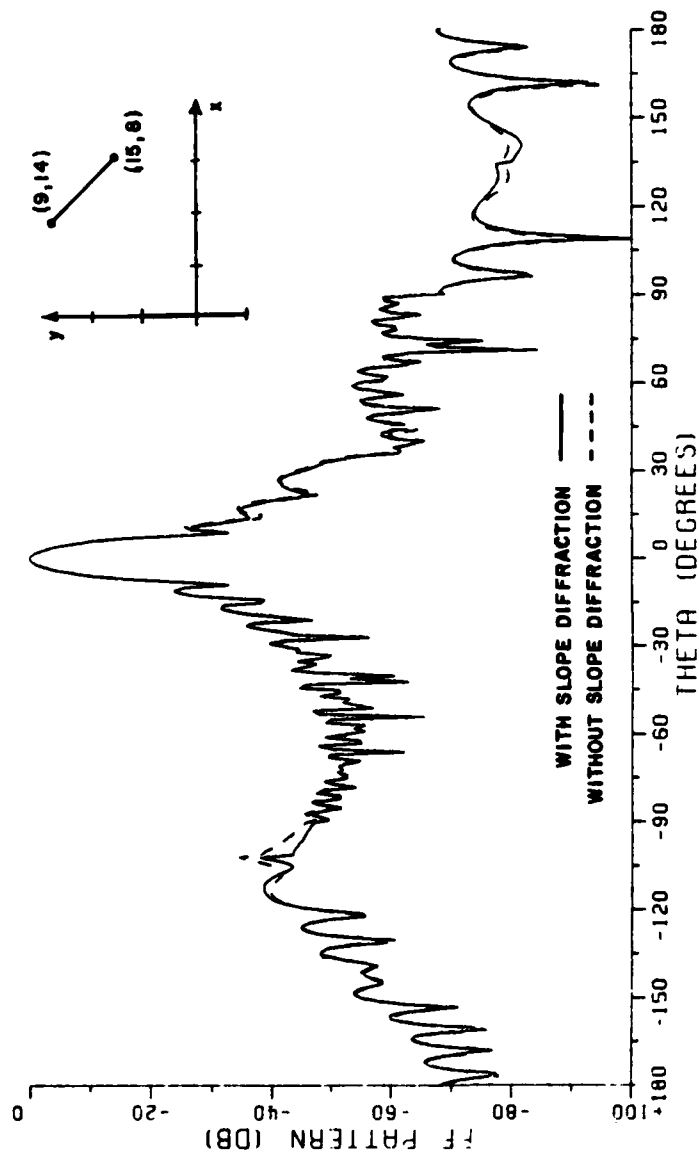


Figure 38. The effect of slope diffraction from the scatterer A for type 2 antenna.

D. Combination of Large Subaperture and Two-point GTD Source Methods

In this section, the results of the previous sections are presented to show the effect of the scatterer. The results were obtained by using two-point GTD method in all regions except the main beam, where the large subaperture method is used. In order to see the effect of the scattering, the source fields without the scatterer present are plotted as dashed lines in Figures 40 to 46. Note that the back source fields for  $|\theta| > 90^\circ$  of the 2-point GTD are kept in this section as shown in Figures 39 and 42. It is clear that each scatterer has its maximum effects near the reflected and blocked regions, which are marked on the figures.

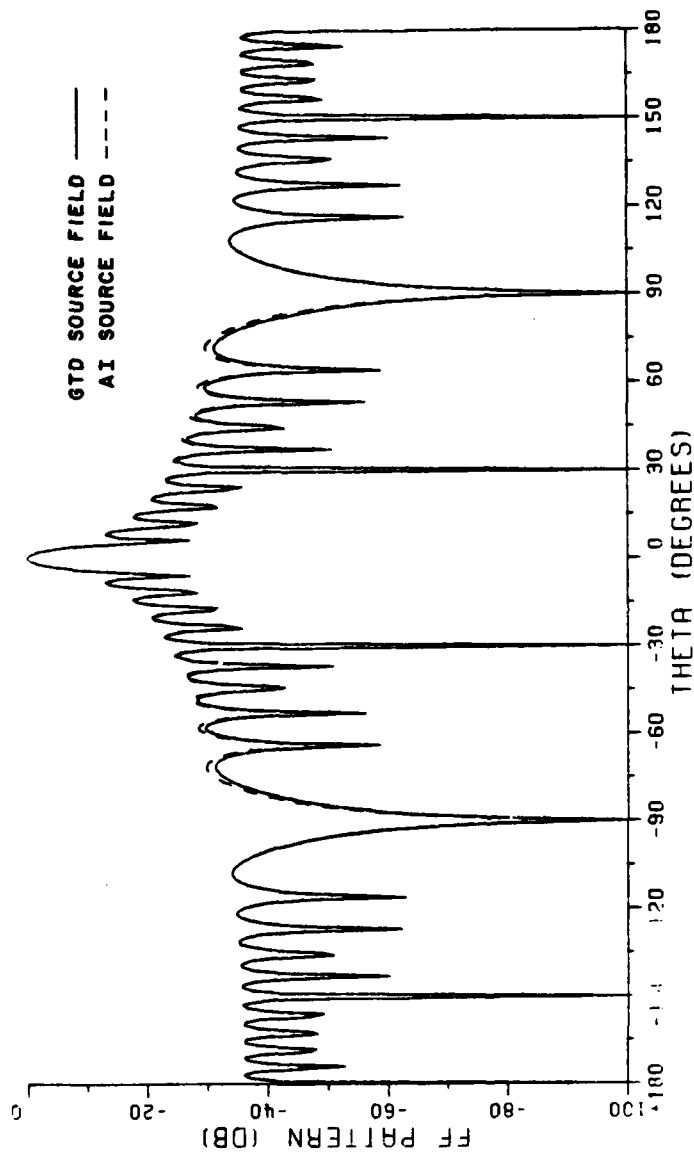


Figure 39. The far field pattern of a  $10\lambda$  type antenna calculated by the two-point GTD method.

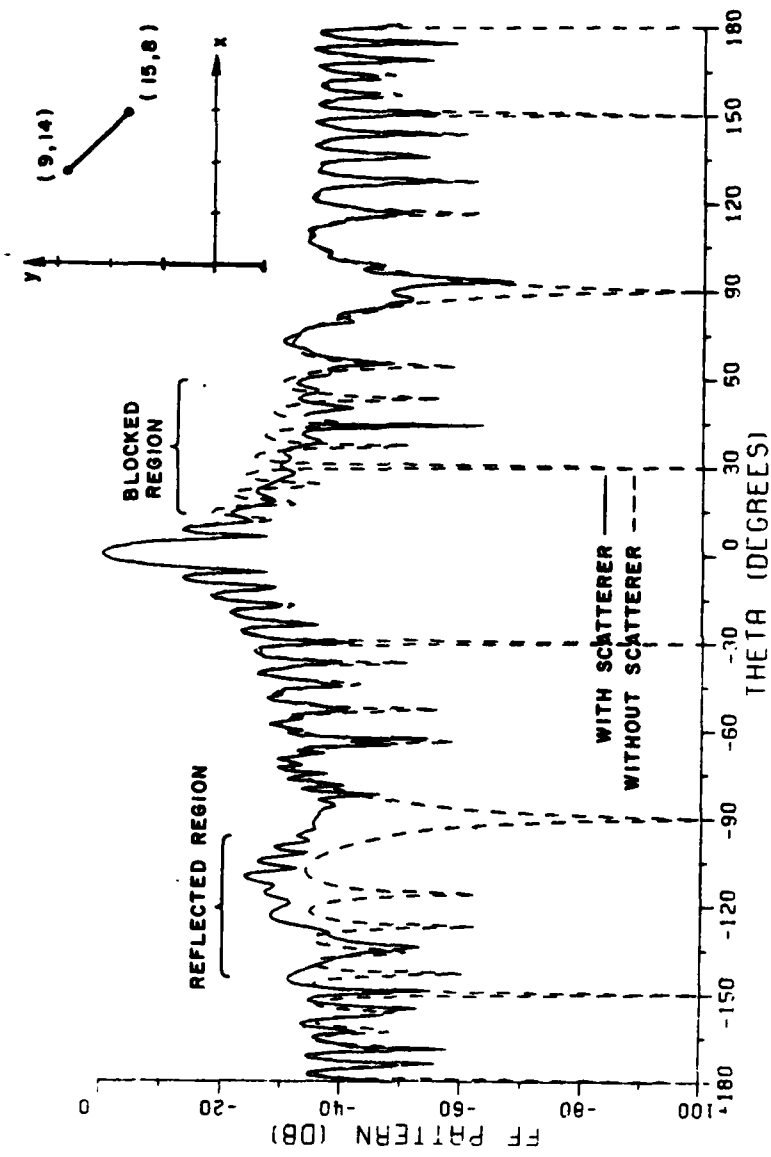


Figure 40. The scattering effect of a 10λ type 1 antenna with scatterer A. Two approaches are combined and compared to the source field.

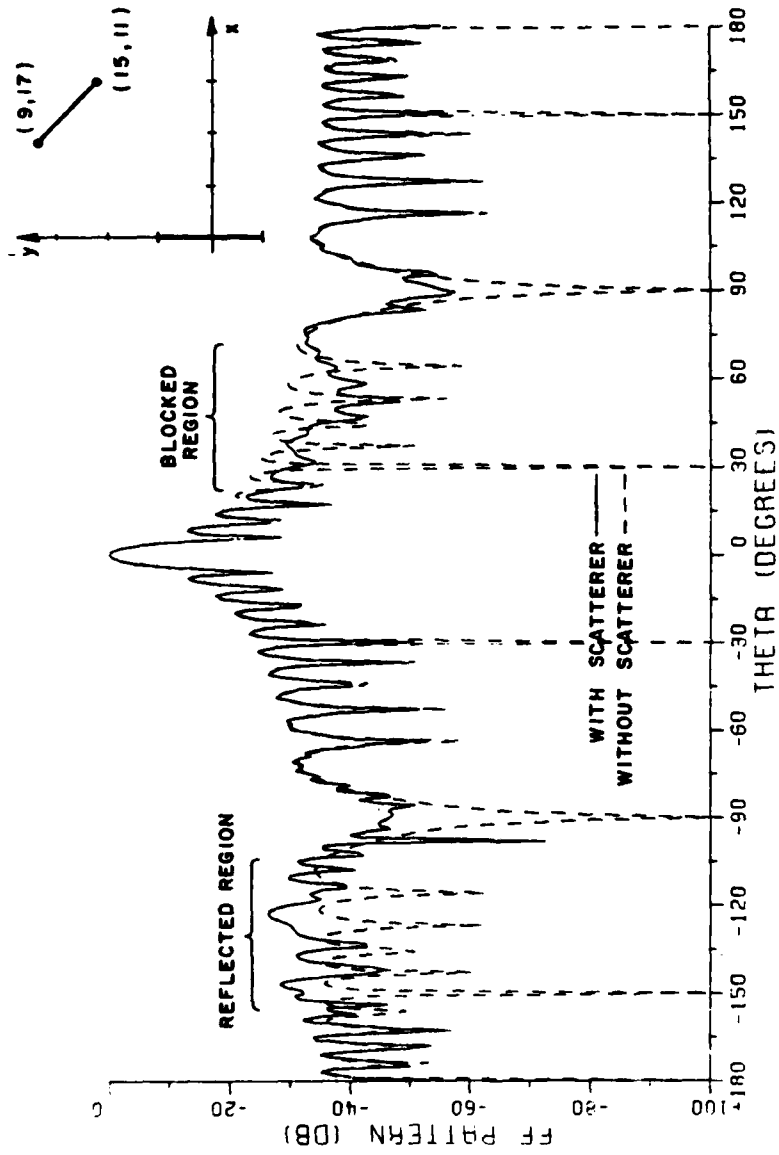


Figure 41. The scattering effect of a  $10\lambda$  type I antenna with scatterer E.

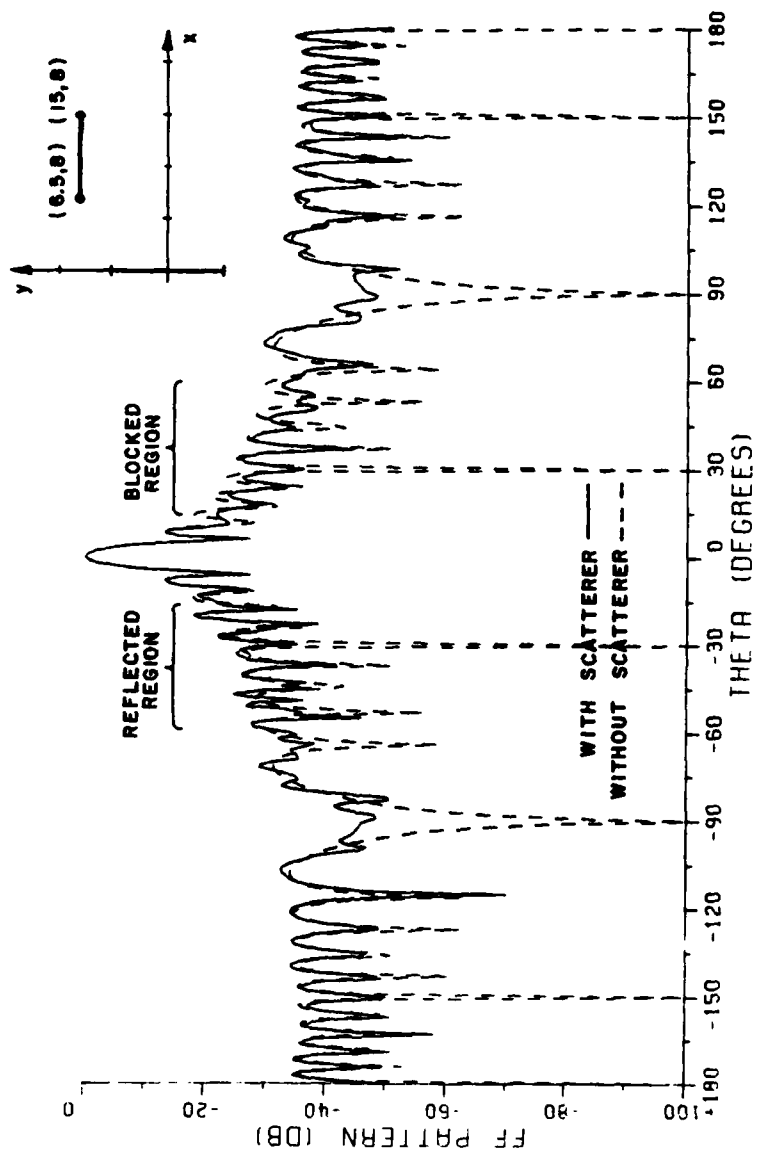


Figure 42. The scattering effect of a  $10\lambda$  type 1 antenna with scatterer B.

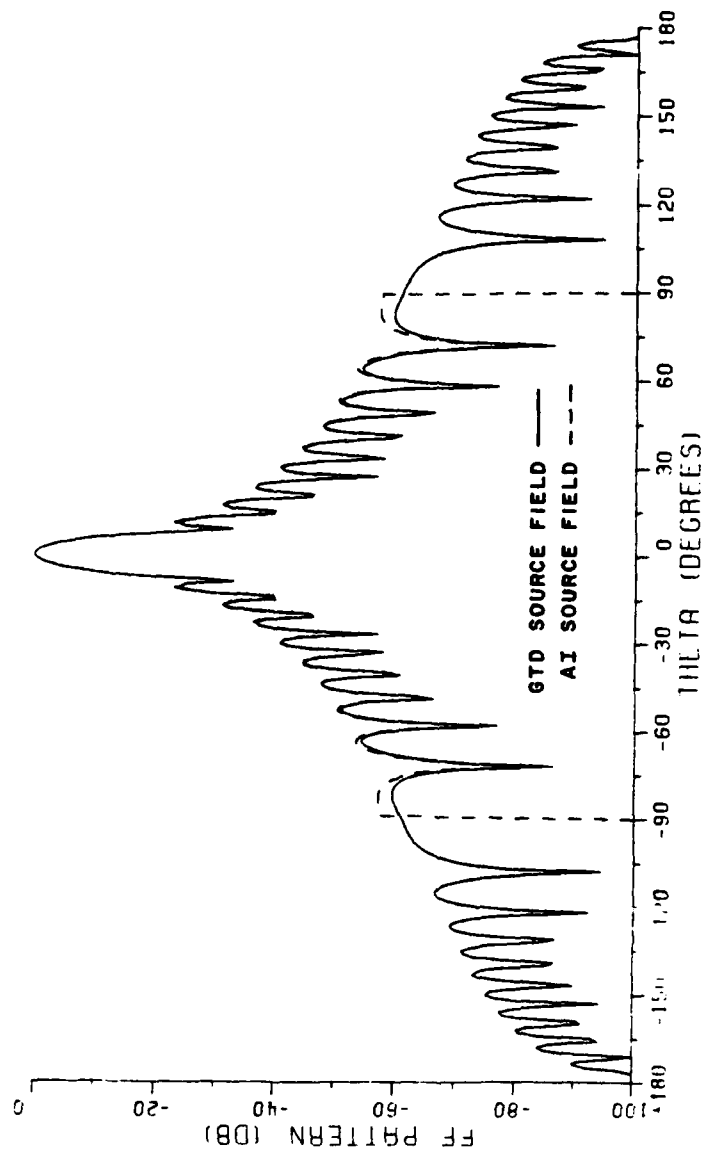


Figure 43. The far field pattern of a  $10\lambda$  type 2 antenna calculated by the two-point GTD method.

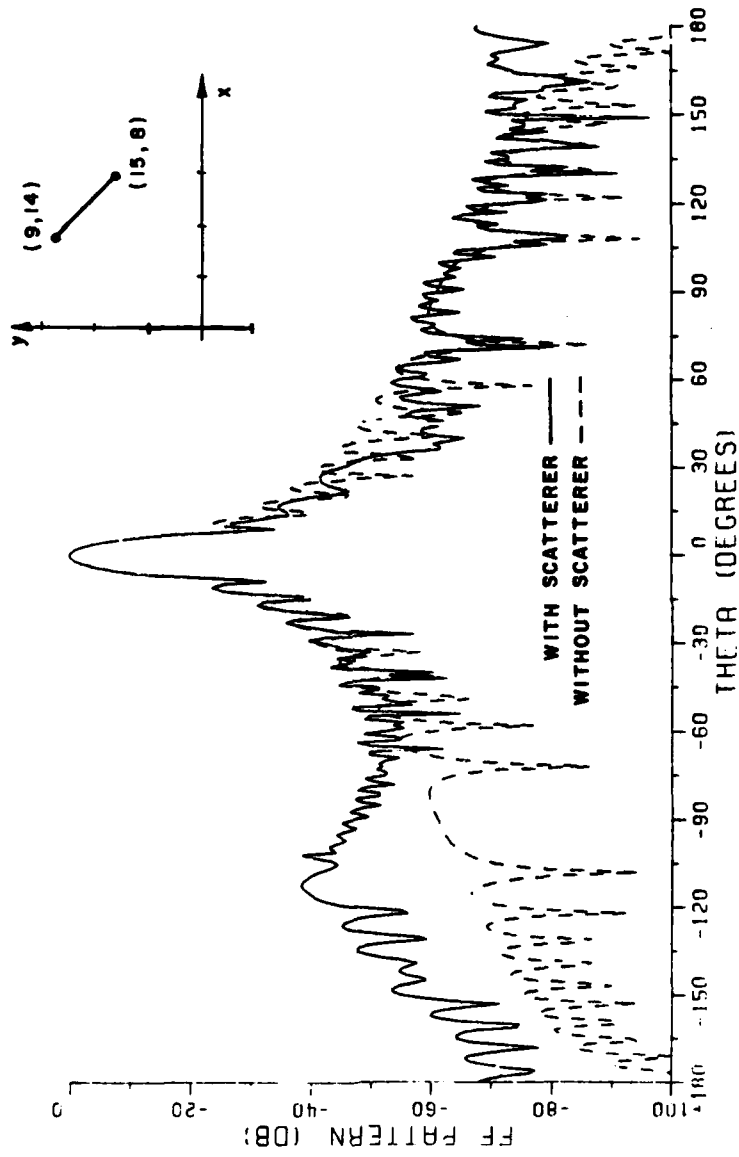


Figure 44. The scattering effect of a  $10\lambda$  type 2 antenna with scatterer A.

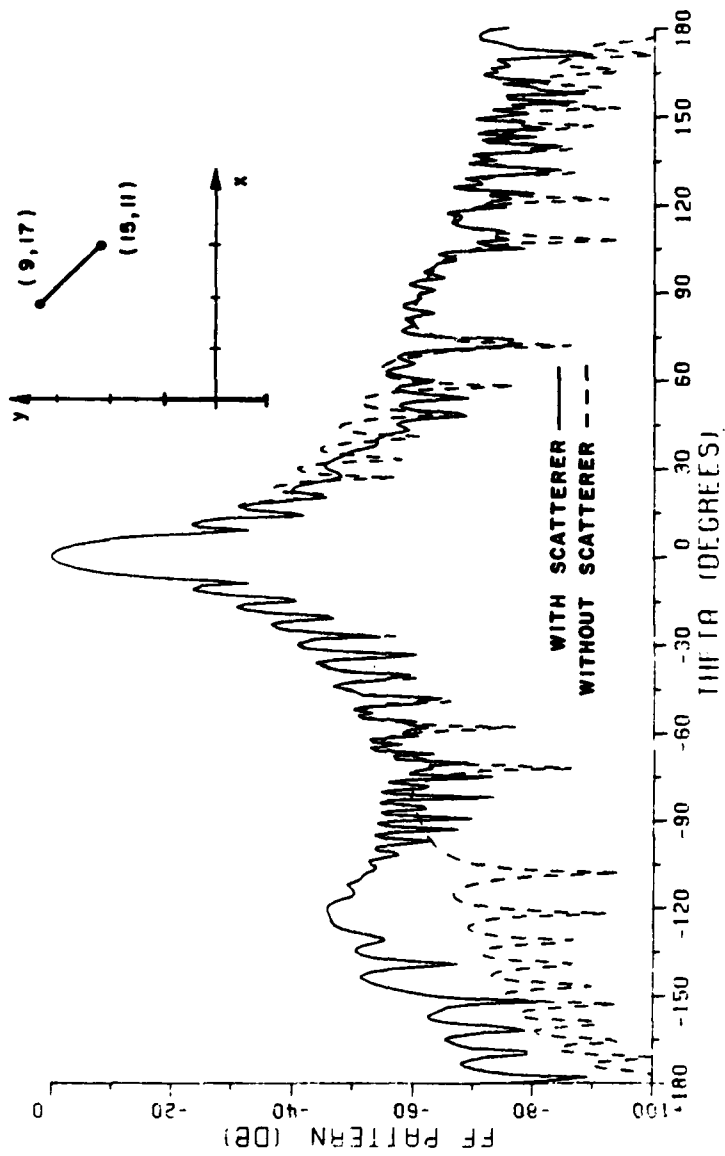


Figure 45. The scattering effect of a  $10\lambda$  type 2 antenna with scatterer E.

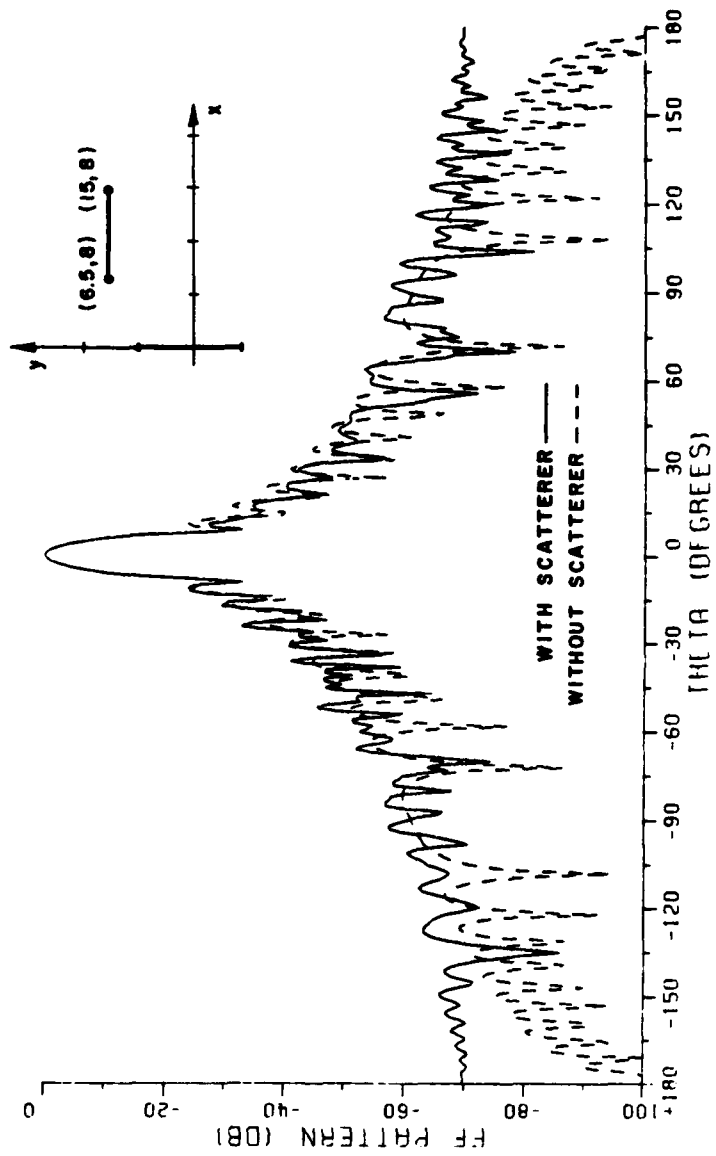


Figure 46. The scattering effect of a  $10\lambda$  type 2 antenna with scatterer B.

CHAPTER VIII  
EXAMPLES OF OTHER APPLICATIONS

In Chapters V and VI, only a normally incident plane wave is considered; however, this is not a necessary condition. In this chapter, some more general cases are considered and two examples are demonstrated as follows:

A. Scanning Mode

The first example is a plane wave incident at an angle  $\theta_m$  for a phase scanned planar array as shown in Figure 47. The diffraction solution is modified in terms of the following angles:

$$\phi_1' = \frac{\pi}{2} - \theta_m, \quad \phi_2' = \frac{\pi}{2} + \theta_m, \quad \phi_1 = \frac{\pi}{2} - \theta, \quad \text{and} \quad \phi_2 = \frac{\pi}{2} + \theta. \quad (8-1)$$

Considering only the  $DI^+$  terms as done previously, one finds

$$\phi_1 + \phi_1' = \pi - (\theta + \theta_m), \quad \text{and} \quad (8-2)$$

$$\phi_2 + \phi_2' = \pi + (\theta + \theta_m),$$

while the remaining terms are the same as those shown in Figure 48. From Equation (5-6), as  $s_1, s_2 \rightarrow \infty$ , the pattern function  $F^S(\theta)$  of the source field is given by

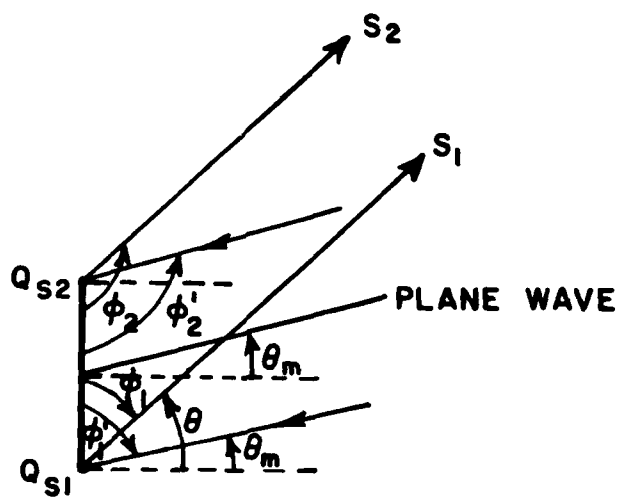


Figure 47. A scanning mode for two-point GTD method.

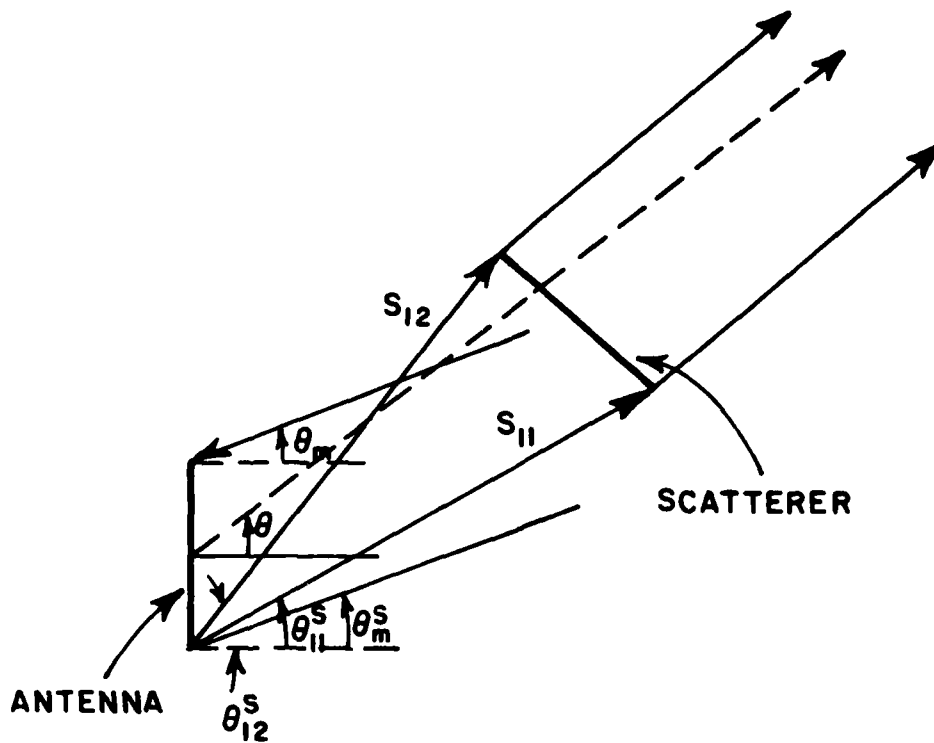


Figure 48. The scanning mode with the scatterer present.

$$F^S(\theta) = E_0 [D_I(s_1, \pi - (\theta + \theta_m)) e^{jky_{s1} \sin \theta} + D_I(s_2; \pi + (\theta + \theta_m)) e^{jky_{s2} \sin \theta}]$$

(8-3)

Note that this equation is obtained from Equation (5-6) by changing  $\theta$  to  $\theta + \theta_m$ .

With the presence of the strip scatterer as shown in Figure 48, the source, reflected, and diffracted fields can be calculated as in section B of Chapter V except that the angles associated with the diffraction coefficients should be changed from  $\theta$  to  $\theta + \theta_m$ , where  $\theta_m$  is the scan angle.

#### B. Cylindrical Wave Radiator

The second example is a line source behind a conducting slot as shown in Figure 49a. The analysis is similar to that used to study horn antennas as done in [8]. This problem can be modeled by a line source located at  $(x_s, y_s)$  in the presence of a perfectly conducting strip as shown in Figure 49b. In this case, the source fields of the strip scatterer include two contributions, one is the geometric optics term  $E_{G,0}$ , and the other is the diffractions from edges  $Q_{s1}$  and  $Q_{s2}$  as discussed previously. Then the total field is the superposition of the fields caused by these two contributions as discussed below.

## 1. Terms Caused by Geometric Optics Source

First, the geometric optics field without the strip scatterer present is given by

$$E^{G.O.} = \begin{cases} \frac{e^{jks'}}{\sqrt{s'}} & \text{for } \theta_m \leq \theta \leq \theta_{m2}, \text{ and} \\ 0 & \text{elsewhere,} \end{cases} \quad (8-4)$$

where  $\theta_{m1}$ ,  $\theta_{m2}$ , and  $s'$  are shown in Figure 50. Then, with the strip scatterer present, the source, reflected, and diffracted fields caused by  $E^{G.O.}$  can be calculated separately as before. Note that depending on the source point  $(x_s, y_s)$  and the location of the scatterer, some of these contributions may not exist. A case in which all the contributions exist is shown in Figure 51a. On the other hand, only the source field and part of the reflected and diffracted exist for the geometry shown in Figure 51b. Finally, an example without any reflected and diffracted fields caused by the geometric optics source is shown in Figure 51c.

## 2. Terms Caused by Diffraction Sources

Next, the contributions due to the source fields caused by the diffractions from  $Q_{s1}$  and  $Q_{s2}$  can be analyzed as before except that  $\phi_1'$ ,  $\phi_2'$ ,  $E^i(Q_{s1})$  and  $E^i(Q_{s2})$  are appropriately modified. The geometry associated with this case is shown in Figure 52, where  $\phi_1'$ ,  $\phi_2'$ ,  $s_1'$  and  $s_2'$  are determined by

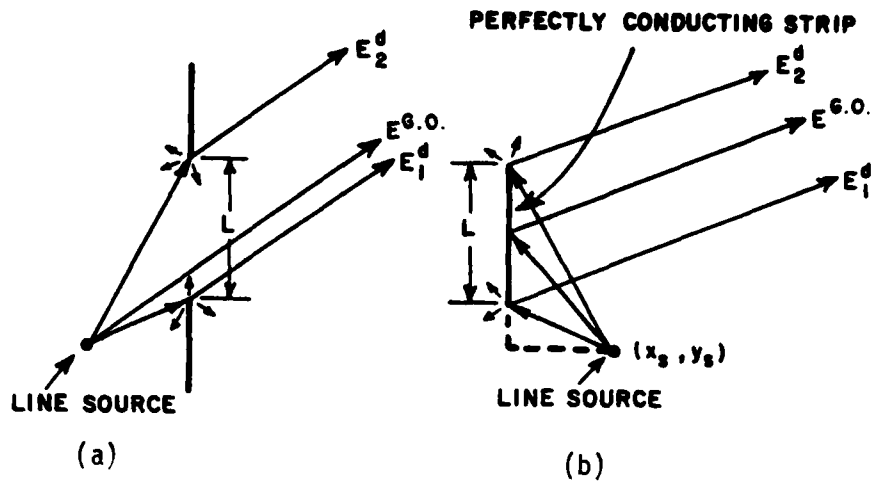


Figure 49. The duality of a line source with a conducting slot and a conducting strip.

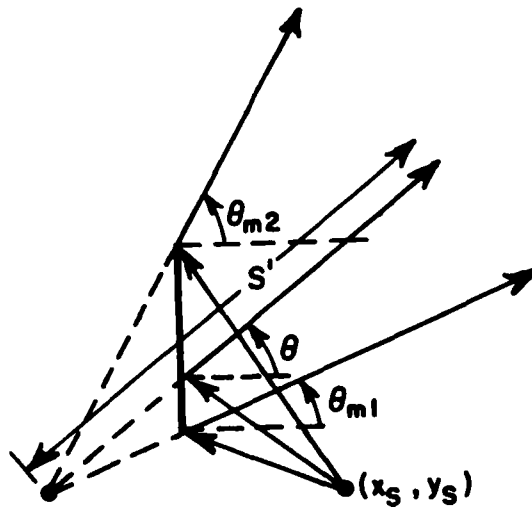


Figure 50. Geometric optics field for antenna.

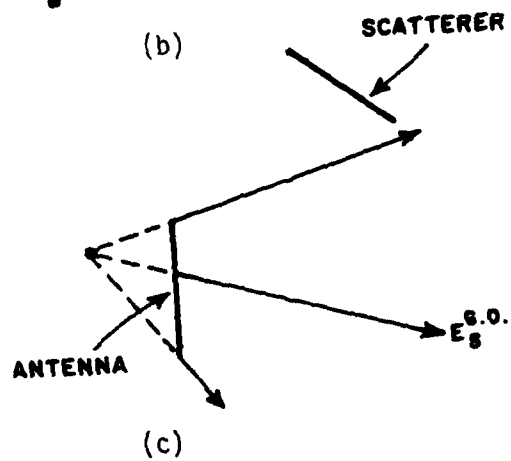
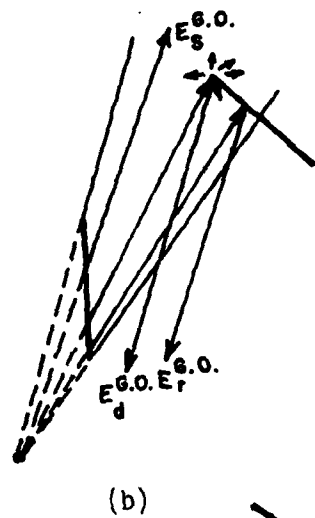
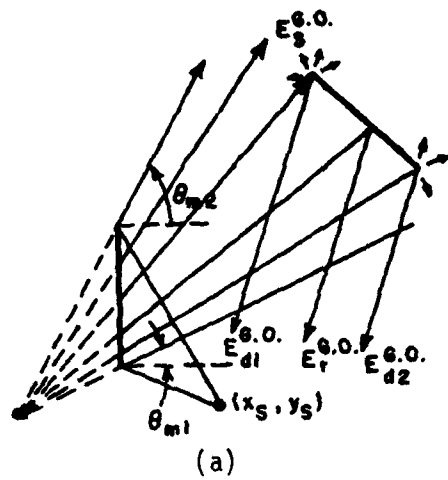


Figure 51. The source, reflected, and diffracted fields caused by the geometric optics field.

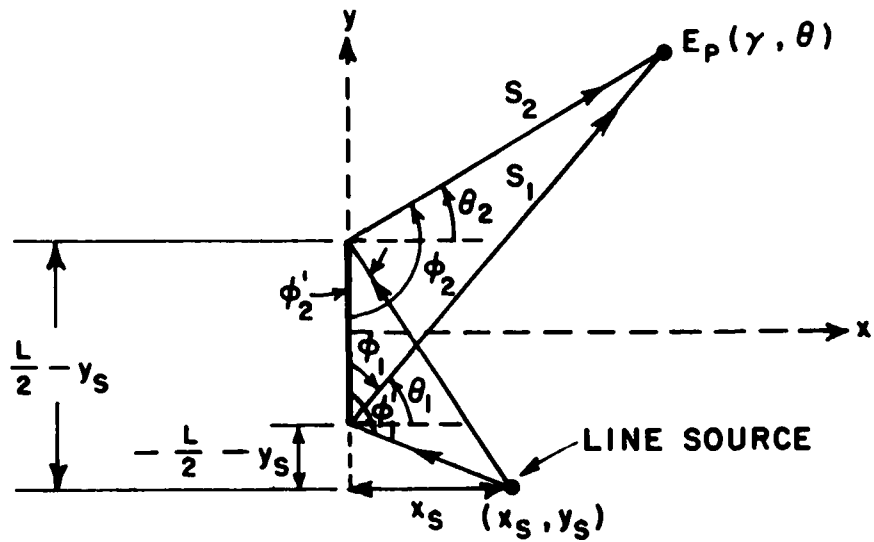


Figure 52. The diffracted field of a line source.

$$s_1' = \sqrt{x_s^2 + \left(-\frac{L}{2} - y_s\right)^2}, \quad (8-5)$$

$$s_2' = \sqrt{x_s^2 + \left(\frac{L}{2} - y_s\right)^2},$$

$$\phi_1' = \frac{\pi}{2} + \tan^{-1}\left(\frac{-\frac{L}{2} - y_s}{x_s}\right), \quad \text{and}$$

$$\phi_2' = \frac{\pi}{2} - \tan^{-1}\left(\frac{\frac{L}{2} - y_s}{x_s}\right). \quad (8-6)$$

Besides, as defined before,  $\phi_1 = \frac{\pi}{2} - \theta_1$  and  $\phi_2 = \frac{\pi}{2} + \theta_2$ . So the source field  $E_p(r, \theta)$  at point P due to the diffraction from  $Q_{s_i}$  given by

$$E_p(r, \theta) = \frac{e^{-jks'_i}}{\sqrt{s'_i}} D_I(L_i; \phi_i + \phi'_i) \frac{e^{-jks_i}}{\sqrt{s_i}} \quad \text{for } i = 1, 2, \text{ and} \quad (8-7)$$

$$L_i = \frac{s_i s'_i}{s_i + s'_i} .$$

If one considers the far field of the source field, that is, when  $r \rightarrow \infty$ , then  $s_1, s_2 \rightarrow \infty$  and  $\theta_1 = \theta_2 = \theta$ . The pattern of the source field becomes

$$F^S(\theta) = \frac{E_0 e^{-jks'_1}}{\sqrt{s'_1}} D_I(s'_1; \phi_1 + \phi'_1) e^{jky_{s1} \sin \theta} + \frac{E_0 e^{-jks'_2}}{\sqrt{s'_2}} D_I(s'_2; \phi_2 + \phi'_2) e^{jky_{s2} \sin \theta} \quad (8-8)$$

Note that it is similar to Equation (5-6) except that  $E^i(Q_{s_i})$  is changed from  $E_0$  to

$$\frac{E_0 e^{-jks'_i}}{\sqrt{s'_i}} .$$

In the presence of the strip scatterer, let  $p$  be  $Q_{Cj}$ , then  $E_i^I$  becomes the incident field  $E_{ij}^I$  from  $Q_{Si}$  to the edge  $Q_{Cj}$ , and the pattern of the diffracted fields from the scatterer are obtained using

$$F^d(\theta) = \sum_{i=1}^2 \sum_{j=1}^2 E_{ij}^I D_{ij} e^{j\psi_{dj}} \quad (8-9)$$

where the diffraction coefficient  $D_{ij}$  and phase factor  $\psi_{dj}$  are defined in Equation (5-15) and (3-12), respectively.

## CHAPTER IX

### CONCLUSIONS

As discussed in Chapter III, GTD can be used to accurately analyze scattering problems. However, the use of the aperture integration source is not efficient, especially when the antenna is large in terms of the wavelength. The large subaperture technique and two-point GTD source field method were studied in this thesis as ways to improve the efficiency, and their corresponding advantages and limitations are shown in the results. From these results, it can be concluded that the subaperture technique works well for  $1\lambda$  subapertures and that it works reasonably well for  $2\lambda$  subapertures except in some small regions for certain cases. Two-point GTD turned out to be a very good approach for both types of aperture distributions (uniform and cosine) in all regions except the main beam as long as the scatterer is not too close to the projected aperture of the antenna.

If the scatterer is near the projected aperture, the slope of the incident field on the edges of the scatterer becomes significant. In this case slope diffractions from the scatterer can be added to improve the accuracy near the shadow boundaries, but it can not solve the problem completely if the scatterer is too close to the projected aperture of the antenna.

AD-A096 600

OHIO STATE UNIV COLUMBUS ELECTROSCIENCE LAB

F/G 20/14

6TD ANALYSIS OF A STRIP SCATTERER IN THE NEAR FIELD OF AN ANTEN--ETC(U)

DEC 80 Y CHANG

N62269-80-C-0384

FSL-713303-1

NL

UNCLASSIFIED

Doc  
No  
Sec



END

DTIC

DTIC

DTIC

DTIC

Since the purpose for developing the two approaches discussed in this thesis was to improve the efficiency of the calculations, consequently the CPU time is another important result to discuss. For the large subaperture technique, the efficiency improvement is approximately proportional to the number of the elements used in one subaperture. That is, if 3 elements are used in one subaperture, it only takes about 1/3 of the original CPU time to calculate the results. For the two-point GTD method, the CPU time is independent of the size of the antenna. For the results shown from Figures 29 to 33, the GTD method is more efficient than using  $\lambda/3$  elements by a factor of about 9 for a  $10\lambda$  source antenna. It is obvious that the efficiency will be even better for larger source antennas.

In this thesis, only a single 2-D strip scatterer was studied. If 3-D cases or multiple strip scatterers are considered, more complicated factors such as corner diffraction, polarization, second order diffraction, etc. should also be considered.

APPENDIX A  
ELEMENT PATTERN USED FOR APERTURE INTEGRATION

As discussed in Chapter V, the radiation pattern of an aperture antenna can be analyzed by using the 2-point GTD method. In this section, a modified Huygen's element pattern  $\cos \theta/2$  is derived by comparing the results from 2-point GTD method and from aperture integration (AI). Using this element pattern in the AI, one gets a good agreement between GTD and AI. By using GTD as shown in Figure A-1, the radiation pattern  $E_{\text{GTD}}$  is given by

$$\begin{aligned}
 E_{\text{GTD}} &= E^i \left[ D_I^+(\pi-\theta) \frac{e^{-jks_1}}{\sqrt{s_1}} + D_I^+(\pi+\theta) \frac{e^{-jks_2}}{\sqrt{s_2}} \right] \\
 &= E^i \left[ D_I^+(\pi-\theta) e^{-\frac{jkL \sin \theta}{2}} + D_I^+(\pi+\theta) e^{\frac{jkL \sin \theta}{2}} \right] \frac{e^{-jkR}}{\sqrt{R}}
 \end{aligned}$$

(A-1)

where  $D_I^+(\pi \pm \theta) = \pm \frac{e^{-j \frac{\pi}{4}}}{2\sqrt{2}\pi k} \frac{F(kLa)}{\sin \theta/2}$

and  $k$  is wave number =  $2\pi/\lambda$

Since  $F(kLa) \rightarrow 1$  for the far field,

$$\begin{aligned}
 E_{GTD} &= \frac{E^i e^{-j\frac{\pi}{4}}}{4\pi \sin \frac{\theta}{2}} \left[ 2j \sin\left(\frac{kL}{2} \sin \theta\right) \right] \frac{e^{-jkR}}{\sqrt{R}} \\
 &= \frac{E^i e^{-j\frac{\pi}{4}}}{2\pi} \cdot \frac{\sin\left(\frac{kL}{2} \sin \theta\right)}{\sin \frac{\theta}{2}} \frac{e^{-jkR}}{\sqrt{R}} .
 \end{aligned} \tag{A-2}$$

On the other hand, by using aperture integration as shown in Figure A-2 and representing the element pattern as  $F_E(\theta)$ , we obtain

$$E_{AI} = C \cdot \int_{-\frac{L}{2}}^{\frac{L}{2}} \frac{e^{-jks'}}{\sqrt{s'}} F_E(\theta) dy' \tag{A-3}$$

where  $C$  is a constant. For the far field,  $s' \approx R - y' \sin \theta$

$$\begin{aligned}
 \therefore E_{AI} &= C F_E(\theta) \cdot \frac{e^{jky \sin \theta}}{jk \sin \theta} \Big|_{-\frac{L}{2}}^{\frac{L}{2}} \cdot \frac{e^{-jkR}}{\sqrt{R}} \\
 &= \frac{C}{2\pi} \cdot F_E(\theta) \cdot \frac{\sin\left(\frac{kL}{2} \sin \theta\right)}{\sin \frac{\theta}{2} \cos \frac{\theta}{2}} \cdot \frac{e^{-jkR}}{\sqrt{R}}
 \end{aligned} \tag{A-4}$$

Using the Huygen's source element pattern as given by

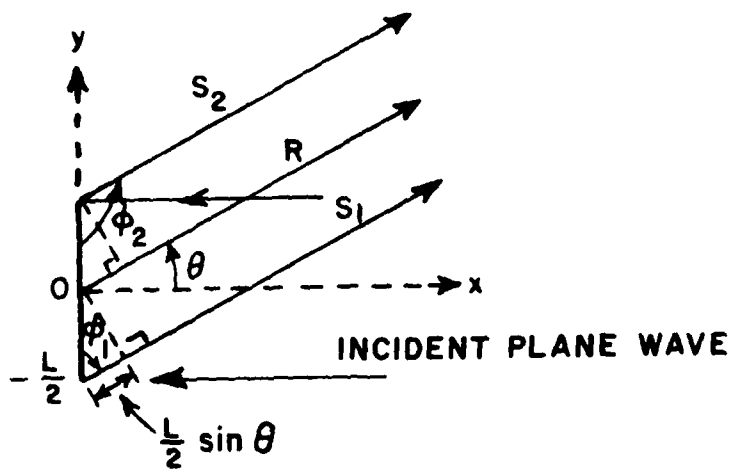


Figure A-1. The two-point GTD method.

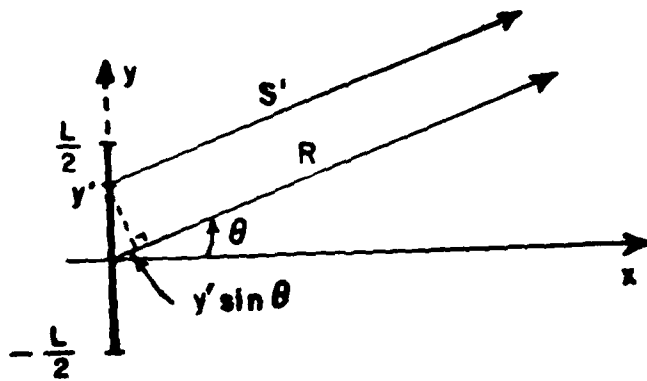


Figure A-2. The aperture integration.

$$F_E(\theta) = \frac{1+\cos\theta}{2} = \cos^2 \frac{\theta}{2} \quad (\text{A-5})$$

results in

$$E_{AI} = \frac{C}{2\pi} \cos \frac{\theta}{2} \cdot \frac{\sin\left(\frac{kL}{2} \sin\theta\right)}{\sin \frac{\theta}{2}} \cdot \frac{e^{-jkR}}{\sqrt{R}} \quad (\text{A-6})$$

However, simple use of a modified Huygen's source

$$F_E(\theta) = \cos \frac{\theta}{2}$$

gives a result which is identical to GTD as follows:

$$E_{AI} = \frac{C}{2\pi} \cdot \frac{\sin\left(\frac{kL}{2} \sin\theta\right)}{\sin \frac{\theta}{2}} \cdot \frac{e^{-jkR}}{\sqrt{R}} \quad (\text{A-8})$$

## REFERENCES

1. R.J. Marhefka, "Analysis of Aircraft Wing-Mounted Antenna Patterns," Report 2902-25, June 1976, The Ohio State University ElectroScience Laboratory, Department of Electrical Engineering; prepared under Grant No. NGL 36-008-138 for National Aeronautics and Space Administration.
2. F.W. Schmidt and R.J. Marhefka, "Numerical Electromagnetic Code (NEC) - Basic Scattering Code, Part II: Code Manual," Report 784508-14, September 1979, The Ohio State University ElectroScience Laboratory, Department of Electrical Engineering; prepared under Contract N000123-76-C-1371 for Naval Regional Procurement Office.
3. R.G. Kouyoumjian and P.H. Pathak, "A Uniform Geometrical Theory of Diffraction for an Edge in a Perfectly-Conducting Surface," Proc. IEEE, Vol. 62, November 1974, pp. 1448-1461.
4. H.H. Chung and R.C. Rudduck, "Near Field Correction Curves for Standard Gain Horn Antennas," Report 711587-1, March 1980. The Ohio State University ElectroScience Laboratory, Department of Electrical Engineering; prepared under Contract N00014-76-A-0039-RZ01 for 2750th Air Base Wing/PMR, Specialized Procurement Branch.

- I
5. S.H. Lee and R.C. Rudduck, "Numerical Electromagnetic Code (NEC) - Reflector Antenna Code: Part II: Code Manual," Report 784508-16, September 1979, The Ohio State University ElectroScience Laboratory, Department of Electrical Engineering; prepared under Contract N00123-76-C-1371 for Naval Regional Procurement Office.
  6. S.H. Lee, "GTD Analysis of Reflector Antenna with General Rim Shapes - Near and Far Field Solutions," Report 712242-4, September 1980, The Ohio State University ElectroScience Laboratory, Department of Electrical Engineering; prepared under Contract N00123-79-C-1469 for Naval Regional Procurement Office.
  7. P.M. Russo, R.C. Rudduck, and L. Peters, Jr., "A Method for Computing E-plane Patterns of Horn Antennas," IEEE Trans. on Antennas and Propagation, AP-13, No. 2, March 1965, pp. 291-224.
  8. R.C. Rudduck and C.L. Chen, "New Plane Wave Spectrum Formulations for the Near-Fields of Circular and Strip Apertures," IEEE Trans. on Antennas and Propagation, Vol. AP-24, No. 4, July 1976, pp. 438-449.
  9. W.D. Burnside and C.S. Kim, "Pattern Analysis of a Horn Antenna in the Presence of Obstacles," Report 711588-1, February 1980, The Ohio State University ElectroScience Laboratory, Department of Electrical Engineering; prepared under Contract N62269-78-C-0379 for Naval Air Development Center.

